A FUSION TRANSMUTATION OF WASTE REACTOR

W. M. STACEY,* J. MANDREKAS, E. A. HOFFMAN, G. P. KESSLER, C. M. KIRBY,
A. N. MAUER, J. J. NOBLE, D. M. STOPP, and D. S. ULEVICH *Georgia Institute of Technology*
Nuclear and Radiological Engineering Program and Fusion Research Center, Atlanta, Georgia 30332

Received May 29, 2001
Accepted for Publication October 5, 2001

A design concept and the performance characteristics for a fusion transmutation of waste reactor (FTWR), a subcritical fast reactor driven by a tokamak fusion neutron source, are presented. The present design concept is based on nuclear, processing, and fusion technologies that either exist or are at an advanced stage of development and on the existing tokamak plasma physics database. An FTWR, operating with $k_{eff} \leq 0.95$ at a thermal power output of ~3 GW and with a fusion neutron source operating at $Q_p = 1.5$ to 2, could fission the transuranic content of ~100 metric tons of spent nuclear fuel per full-power year and would be self-sufficient in both electricity and tritium production. In equilibrium, a nuclear fleet consisting of light water reactors (LWRs) and FTWRs in the electrical power ratio of 3/1 would reduce by 99.4% the actinides discharged into the waste stream from the LWRs in a once-through fuel cycle that must be stored in high-level waste repositories.

KEYWORDS: *fusion transmutation, spent fuel, fusion neutron source*

I. INTRODUCTION

There is a substantial worldwide research and development (R&D) activity devoted to the transmutation of spent nuclear fuel[1–3] (SNF). The objective of this activity is to technically evaluate the possibility of reducing the requirements for long-term geological repositories for the storage of high-level radioactive waste from SNF by neutron fission of the plutonium and higher actinides remaining in the spent fuel discharged from fission power reactors. Repeated recycling of this spent fuel in commercial thermal spectrum fission power reactors would not significantly reduce the repository requirements, because the destruction of actinides by fission would be offset by the production of actinides by neutron capture in ^{238}U (Refs. 1 and 2). Repeated recycling of the spent fuel in special purpose fast spectrum reactors could reduce the radiotoxicity of the SNF by a factor of ~100, limited by safety and criticality constraints.[1] These constraints could be relaxed if the reactors (fast or thermal spectrum) could be operated subcritically, which would require a neutron source. There is a general consensus that significantly higher levels of actinide destruction can be achieved by repeated recycling of spent fuel in subcritical reactors with a neutron source. An accelerator-spallation neutron source has been extensively studied for this application.[1–6]

Deuterium-tritium (D-T) fusion neutron sources could also be used to drive subcritical reactors for the destruction of actinides, and a few scoping studies[7–13] have been carried out. In particular, Ref. 13 reviewed the requirements for a neutron source vis-à-vis the present tokamak database and found that the physics parameters routinely achieved in operating tokamaks ($H \approx 1$, $\beta_N =$ 2 to 3) and operation at Q_p as low as 1.5 to 2.0 would be sufficient for a tokamak neutron source with major radius $R = 3$ to 5 m to produce transmutation rates of hundreds to thousands of kg/FPY (full-power year) of SNF in a subcritical transmutation reactor.

Our purposes in this paper are to identify the physical and performance characteristics of a subcritical transmutation reactor driven by a tokamak fusion neutron source at the lower end of this range of sizes and performance capabilities. The general design objectives for this fusion transmutation of waste reactor (FTWR) are that it (a) destroy the transuranic content of hundreds of metric tonnes/FPY of SNF, (b) utilize nuclear and processing technologies that either exist or are under development, (c) operate at a neutron multiplication factor $k_{eff} \leq 0.95$ to enhance safety, (d) be based on the existing tokamak plasma and fusion technology databases to the maximum extent possible, and (e) be self-sufficient in tritium and electricity production. In this initial effort, we concentrate on those aspects of the design that most influence the configuration and performance characteristics.

*E-mail: weston.stacey@me.gatech.edu

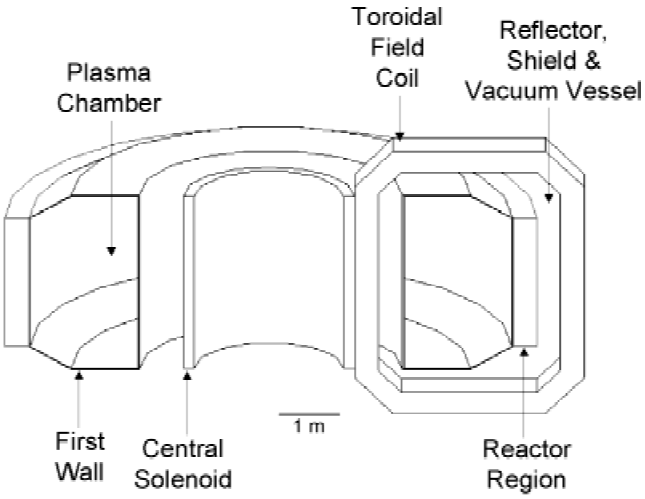

Fig. 1. Schematic of geometric configuration of FTWR.

TABLE I

Materials Composition of FTWR

Component	Material
Reactor	
Fuel	Zr-transuranic alloy in Zr matrix
Clad and Structure	HT-9-like steel
Coolant	Li17Pb83 (^{6}Li enrich 20%)
Reflector	HT-9, Li17Pb83
Shield	HT-9, Li17Pb83, B_4C
Magnets	
Conductor	OFHC
Coolant	LN_2
Structure	Steel
First wall and divertor	
Structure	HT-9-like steel
Coolant	Li17Pb83

II. DESIGN SUMMARY

II.A. Geometric Configuration and Materials

The geometric configuration of the FTWR is shown in Figs. 1 and 2. The transmutation reactor consists of an ≈40-cm-thick ring of vertical hexagonal fuel assemblies located outboard of the plasma chamber of the tokamak fusion neutron source. The reactor metallic fuel consists of a zirconium alloy containing transuranics from SNF dispersed in a zirconium matrix and clad with a steel similar to HT-9. The coolant for the reactor, reflector and shield, first wall, and divertor is Li17Pb83 eutectic enriched to 20% ^{6}Li to meet the tritium self-sufficiency requirement. The reflector and shield are located inboard of, above, and below the plasma chamber and above, below, and outboard of the reactor to protect the magnets from radiation damage and to reflect neutrons toward the reactor. The toroidal and poloidal magnets employ oxygen-free high conductivity (OFHC) copper conductor and liquid nitrogen (LN_2) coolant. The materials composition of the FTWR is summarized in Table I.

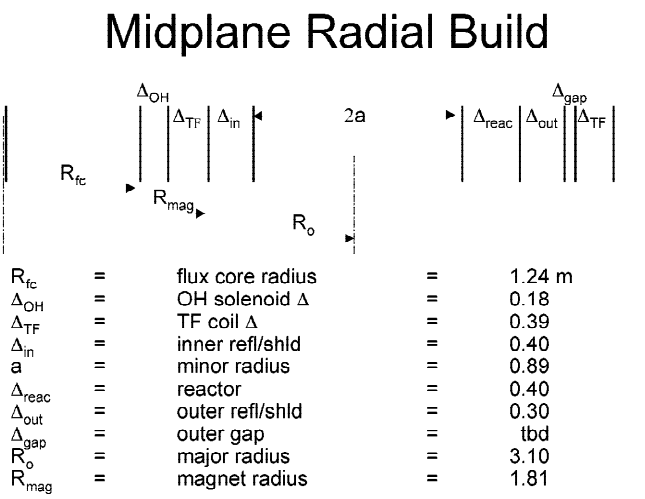

Fig. 2. Radial build of FTWR.

II.B. Major Design Parameters

The neutron source is a D-T tokamak with the parameters shown in Table II, most of which are in the range routinely achieved on operating tokamaks.[14] The only two parameters that fall outside this range are the plasma energy amplification factor Q_p and the steady-state pulse length. The required value of Q_p is only a factor of ~2 greater than what has been achieved on the Joint European Torus (JET) device, and there is a proposal for $Q_p \approx 2$ operation in JET. Perhaps the greatest advance beyond the present state of the art in tokamak operation is the steady-state pulse length. Using a conservative estimate of a current drive efficiency $\eta_{CD} = 0.03$ A/W, we estimate that steady state could be achieved with $Q_p = 1.55$, at 150 MW fusion power. If advances in tokamak R&D (Ref. 15) enable achievement of $\eta_{CD} = 0.05$ to 0.06 A/W or a higher bootstrap current fraction, it should be possible to achieve steady-state pulse length at the reference value of $Q_p = 2$.

The FTWR magnetic system is based on existing technology. The magnetic field levels are well within the range of existing tokamaks. The joule heating and, even more, the LN_2 refrigeration for the resistive magnets constitute the major electrical power requirement for the

TABLE II

Neutron Source Parameters

Parameter	Value
Plasma	
Major radius, R_0 (m)	3.1
Minor radius, a (m)	0.89
Elongation, κ	1.7
Magnetic field, B_0 (T)	6.1
Plasma current, I_p (MA)	7.0
Bootstrap current fraction	0.38
Normalized beta, β_N (%)	2.5
Confinement factor, H-ITER IPB98(y,2)	1.1
Fusion power [MW(thermal)]	150
Plasma energy amplification, Q_p	2.0
Pulse length	Steady state
Magnets	
TF at coil (T)	10.45
CS field at coil (T)	8.0
Inductive flux (V·s)	90
Temperature (K)	80 to 100
Power dissipation and refrigeration [MW(electric)]	972
Lifetime radiation dose (rads)	1.5×10^{12}
Lifetime fast neutron dose (n/cm^2)	1.8×10^{22}
First wall	
14-MeV neutron wall load (MW/m^2)	0.79
Surface heat load (MW/m^2)	0.34
Radiation damage (dpa/623-day cycle)	21
Tritium inventory	
BOC (g)	120
Maximum (g)	1000

FTWR. The lifetime radiation and neutron doses to the toroidal field (TF) coils are intended to be at the limit for ceramic insulators, and may be beyond the limit for organic insulators, although these limits are not well defined. The poloidal coil system [central solenoid (CS) plus ring coils] is designed to provide adequate volt-seconds for inductive startup and a minute or so of burn.

The FTWR first-wall design is an adaptation of the ITER design,[16] albeit with HT-9-like steel structure. Although the qualification of HT-9-like steel for operation in a neutron irradiation environment is in progress, the radiation damage limit is not yet known. However, we believe that this limit will probably allow ~5 to 10 (623-day) cycles (>100 to 200 dpa) before it is necessary to replace the first wall of the neutron source.

The main parameters of the transmutation reactor are given in Table III. The design is an adaptation of the Argonne National Laboratory (ANL) design of a transmutation reactor for an accelerator (ATW) neutron source,[17] which has a fast neutron spectrum to maximize the fission probability per neutron absorbed in transuranics.

TABLE III

Transmutation Reactor Parameters

Parameter	Value
Maximum multiplication constant, k_{eff}	0.95
Actinide loading (MT)	27
Maximum actinide enrichment (V/O)	45
Number of hexagonal fuel assemblies	470
Fuel assembly pitch (cm)	16.1
Fuel assembly length (cm)	228
Fuel pin diameter (cm)	0.635
Average power density (kW/ℓ)	124
Fuel cycle	4 batch
Clad irradiation at discharge (dpa)	150
Coolant T_{in}/T_{out} (K)	548/848
Coolant flow velocity (m/s)	0.76
Coolant mass flow rate (kg/s)	51 630
Coolant pumping power [MW(electric)]	131

II.C. Performance Summary

The performance of the FTWR is summarized in Table IV. An FTWR operating at 3000 MW(thermal) can destroy the transuranic content of ~100 metric tons of SNF per FPY. By repeatedly recycling the unburned FTWR fuel and using transuranics from light water reactor (LWR) SNF as the makeup material, the equilibrium FTWR fuel cycle would ultimately result in an effective reduction in the waste streams of 99.4% of the transuranics discharged from an LWR in the once-through cycle (OTC). While mass alone does not characterize the high-level waste repository requirements, this reduction in mass provides some indication of the corresponding reduction in high-level waste repository requirements. A single 3-GW(thermal) FTWR [3 GW(thermal)] with 60% availability can transmute the transuranic content of the SNF produced in three typical LWRs [1 GW(electric)].

TABLE IV

Major Performance Parameters of FTWR

Parameter	Value
Total power [MW(thermal)]	3000
Thermal-to-electrical conversion (%)	40
Fusion neutron source strength (number/s)	5.32×10^{19}
SNF transmutation rate (MTU/FPY)	102
Transuranic mass reduction in SNF (%)	99.4
Support ratio [GW(electric) LWR/FTWR]	3
Electrical power amplification, Q_e	>1
Lifetime (FPY)	40
Availability (%)	60

The toxicity (defined as the volume of water required to dilute the SNF to the maximum permissible concentration for human consumption) of the original SNF from a once-through LWR cycle and the toxicity from the same SNF after transmutation in an FTWR (without the uranium, which is assumed to be recovered and disposed of as low-level waste in both cases) are compared with the toxicity of the original as-mined uranium ore from which the fuel was fabricated in Fig. 3. The toxicity of the LWR SNF including the uranium is also shown to illustrate the effect of just removing the uranium from the SNF. The SNF from the LWR becomes less toxic in ~7500 yr than the natural as-mined uranium ore from which it was fabricated. If this same SNF were irradiated in the FTWR, it would become less toxic in ~500 yr than the natural as-mined uranium ore from which it was fabricated. While toxicity is only one of many measures of the hazard potential of radioactive waste, this comparison does indicate the magnitude of the benefit of the transmutation of SNF.

At 3 GW(thermal), an FTWR is just self-sufficient in electrical power production (i.e., $Q_e \approx 1$). The principal electrical power requirement is associated with refrigeration of the LN_2 that is required to remove the joule heating from the magnets. If the FTWR design was extended to produce 6 GW(thermal) by increasing the number of fuel assemblies, the power requirements would increase slightly and the electrical power amplification factor would become $Q_e \approx 1.8$, which would allow ≈1-GW(electric) surplus electricity to be produced, as well as doubling the transmutation rate and number of LWRs supported by a single FTWR.

III. DESIGN TRADE-OFF STUDIES

The size and geometry of a subcritical reactor driven by a tokamak fusion neutron source are determined by the size and geometry of the tokamak neutron source and by the transmutation rate (power level) and power density of the surrounding subcritical transmutation reactor. The design objective of identifying the "minimal" tokamak neutron source that would produce a relevant transmutation rate in a subcritical ($k_{eff} \leq 0.95$) reactor and produce electrical power self-sufficiency led to the selection of copper (rather than superconducting) magnets at the outset. The choice of materials was strongly influenced by the design objective of using fusion, nuclear, and processing technologies that either existed or are well along in their development.

III.A. Tokamak Neutron Source Physics Constraints

The standard design methodology used in the ITER design studies, where the major parameters of the machine (R_0, a, I_p, B_0, etc.) are determined by a relatively small number of equations and assumptions,[14,18] was employed. The starting point of this approach is a simple equation for the radial build of the reactor,

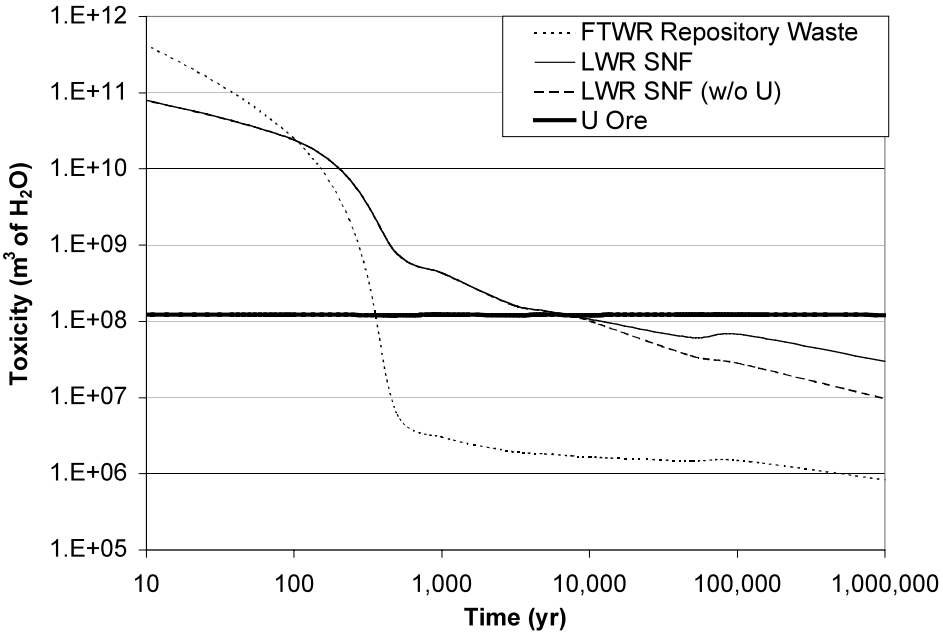

Fig. 3. Toxicity of SNF (uranium recovered) with and without transmutation in FTWR compared to toxicity of natural uranium ore.

$$R_0 = R_{mag} + \Delta_{in} + a \ , \qquad (1)$$

where

R_{mag} = major radius at the inner leg of the TF coil

Δ_{in} = thickness of the inner shield and reflector region between the plasma and the TF coil

a = minor radius (see Fig. 2).

Using Eq. (1) along with expressions for the edge safety factor q_{95}, the beta limit and the Greenwald density limit, taking into account the $1/R$ dependence of the toroidal magnetic field, and assuming that the plasma energy confinement time τ_E is described by one of the usual confinement scalings such as the ITER IPB98$(y,2)$ scaling,[19] an equation can be derived coupling the performance characteristics of the reactor to its major geometric and operational parameters:

$$\frac{(nT\tau_E)_\infty}{1+\dfrac{5}{Q_p}} = F(\beta_N, G_n, \kappa, \delta, q_{95}, \Delta_{RS}, H, A, I_p, B_{TF}, \ldots) \ , \qquad (2)$$

where $(nT\tau_E)_\infty$ is the value of the triple product $nT\tau_E$ required for ignition (usually taken to be equal to 5×10^{21} m$^{-3}\cdot$keV$\cdot$s for D-T reactors), $Q_p = P_{fus}/P_{aux}$, and F is a nonlinear function of various operating and constraint parameters (see Appendix A). If we select reasonable values for the shape parameters and constraint limits δ, κ, q_{95}, β_N, and G_n, and aspect ratio A, we can use Eq. (2) to perform trade-off studies between the size and the major operational parameters (plasma current and maximum TF), for given performance requirements (Q_p and H). An example of such a trade-off study is shown in Fig. 4, where the major parameters of the reactor are plotted versus the maximum toroidal field at the inside leg of the TF coil for a reasonable set of assumptions and performance requirements ($\delta = 0.4$, $\kappa = 1.7$, $q_{95} = 3$, $\beta_N = 2\%$, $G_n = 0.75$, $A = 3.47$, $\Delta_{in} = 0.4$ m, and $Q_p = 5$).

It should be emphasized here that while most of the physics constraints are inequalities ($\beta_t \le \beta_{max}$, etc.), they are treated as equalities in our analysis. This means that the performance and power output of the reactor designs obtained via this procedure are the maximum attainable under the assumed constraints. Once the major reactor size parameters (a, R_0, etc.) are fixed, a wide operating space with more modest performance (Q_p) and fusion powers can be identified by selecting appropriate operating densities and temperatures, or even reducing the plasma current and the toroidal magnetic field.

Based on the results shown in Fig. 4 and on other similar analyses, a major radius of ~3.1 m, corresponding to a maximum field of 14 T at the TF coil and a plasma current of 9.4 MA, was selected for our initial design point. More detailed considerations of the performance characteristics vis-à-vis the neutron source requirements led us to a reference design point with the same size ($R_0 = 3.1$ m, $A = 3.47$) but lower field at the TF coil and lower plasma current (10.4 T and 7 MA, respectively). This choice represents a reasonable trade-off between low cost (small size and low current) and reasonable joule heat removal requirements for the TF system.

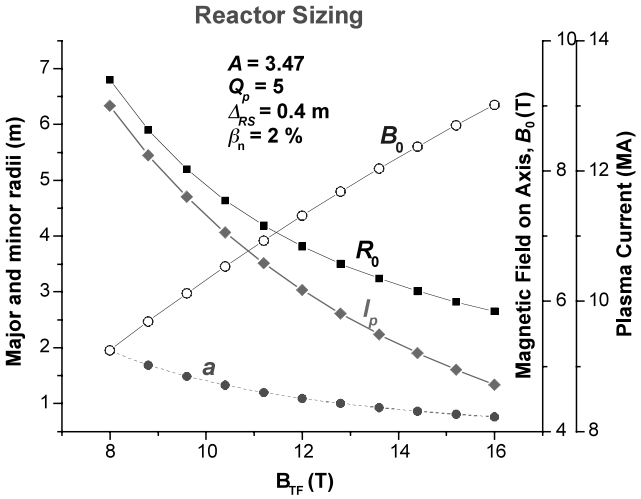

Fig. 4. Various reactor parameters (R_0, a, B_0, I_p) versus the maximum toroidal field at the coil, B_{TF}, for a set of fixed shape and performance parameters.

III.B. Magnet Conductor and Coolant

The selection of the magnet technology, materials, and magnet cooling options was among the most significant design choices we had to make. While most recent steady-state power producing tokamak reactor designs rely on superconducting magnets to minimize the high joule losses associated with resistive magnets, we opted to trade off recirculating power for simpler technology and smaller size (superconducting magnets require a thicker shield, which leads to a larger reactor size, since they are more sensitive to nuclear heating and irradiation). Such a choice of magnet technology would not have been viable for a stand-alone power producing fusion reactor (the total power required to operate and cool the resistive magnets is several times the reference fusion power output of the neutron source), but since in the FTWR most of the useful power originates in the fission (transmutation) part of the system, it is an acceptable trade-off.

Several copper alloys were considered for the magnet conductor, including OFHC copper and beryllium copper (BeCu). OFHC copper, strengthened by steel support, was selected because of its lower resistivity, even though BeCu has better structural properties.

The choice of a coolant for the magnets was also a critical part of the design. Water was considered but rejected, since the resulting Joule heating power was very large (~1.3 GW) due to the high resistivity of copper at the high operational temperatures (~450 K) of the magnets with water coolant. It was decided to use LN_2 to cool the magnets to cryogenic temperatures (~80 to 100 K), because the copper resistivity drops substantially at these temperatures, resulting in substantially reduced joule losses (~110 MW). Although the power required to refrigerate the magnets for steady-state operation is considerable, overall the cryogenic option was more attractive than the water-cooled one.

III.C. Transmutation Reactor Technologies

One of the design objectives was to use to the maximum extent possible nuclear and processing technologies that exist or are being developed. Metal fuel with HT-9-like steel clad and pyrolytic processing technology have been under development at ANL for the fast reactor program for a number of years and have been adopted for further development in the U.S. ATW program.[6] Moreover, a fast neutron spectrum maximizes the transmutation rate per neutron absorbed in actinides. Thus, we use HT-9-like steel clad and metal fuel, following the ATW design.[17]

We considered two coolants, a lead-bismuth eutectic (LBE) and a lead-lithium eutectic. The LBE ($Pb^{45.5}Bi^{55.5}$) has been used in the Soviet nuclear submarine program and is currently under development for the ATW program.[6] We decided to incorporate lithium within the circulating coolant rather than as a solid component to achieve continuous tritium recovery, which would necessitate the addition of lithium to the LBE. There is also a significant development program for the lead lithium eutectic (Li17Pb83) for fusion applications, primarily in Europe.[20]

The physical properties of lithium lead eutectic and lead bismuth eutectic are quite different (see Appendix B). LBE has a much lower melting point, 397 K, than does LiPb, 508 K. However, in general, the other properties of LiPb are far more favorable than those of LBE. The specific heat of LiPb is nearly 50% greater than for LBE. This results in a requirement for much higher flow velocities with the LBE coolant, which, only partially compensated by the lower electrical conductivity of LBE, would require a significantly larger magnetohydrodynamic (MHD) pumping power for LBE than for LiPb. Furthermore, since the LBE would have to be doped with lithium in order to produce the required tritium, the properties of this new alloy may vary significantly from those of LBE, requiring substantial further development. It was found that even at 100% ^{6}Li, as much as 2% lithium would have to be added to the LBE. At more reasonable ^{6}Li enrichments, this value could easily exceed 5%. Therefore, Li17Pb83 was chosen as the primary coolant.

III.D. Reflector and Shield

The magnets must be shielded to protect against radiation damage effects of the fusion neutrons, fission neutrons, and secondary gammas. The blanket region surrounding the plasma will necessarily consist of a first wall and vacuum vessel that are designed based primarily on structural, not shielding, considerations. An additional region must be added to reduce the damage rates to an acceptable level. Furthermore, to enhance the transmutation rate, a reflector is needed to redirect neutrons heading away from the transmutation reactor. The reflector and shield compositions from the ANL ATW design study[17] were adopted. We found that we might be able to design a pure shield as small as 25 cm, but then we would need a relatively large heavy metal loading and ^{6}Li enrichment. On the other hand, using only a reflector, with no shield, would require a reflector thickness of 40 cm. We chose a combined reflector-shield with a thickness of 30 cm, which provided adequate shielding and sufficient tritium production at a reasonable ^{6}Li enrichment, and beyond which no significant further reduction in heavy metal loading could be obtained. We allowed an extra 10 cm for gaps or additional shielding on the inboard. Since the plasma is shifted outward, we did not otherwise allow for a gap between the circular plasma in our model and the wall on the inboard side.

IV. NEUTRON SOURCE PLASMA PHYSICS ANALYSIS

IV.A. Reference Plasma Parameters and Neutron Source Performance

Based on the methodology outlined in Sec. III and taking into account the neutron source requirements of the subcritical fission reactor, an $R_0 = 3.1$-m design with a 7-MA current and a 6.1-T central magnetic field was selected as the FTWR reference design point. While our trade-off studies had assumed a 14-T field at the toroidal coil and $Q_p = 5$ (Fig. 4), subsequent simulations and concerns about the impact of the resistive losses in the TF coil system on the recirculating power of the plant led us to adopt a less demanding set of magnet and performance parameters, namely $B_{TF} = 10.45$ T and $Q_p = 2$, for the reference design point. The major plasma-related parameters of the reference design point are listed in Table V.

A Plasma Operating Contour (POPCON) was constructed for the reference design to help us select an appropriate operating point and to scope out the operating range of the machine. It can be seen from Fig. 5 that an operating point with $Q_p = 2$ and $P_{fus} \approx 150$ MW,

TABLE V

Reference Plasma Parameters of the Fusion Neutron Source

Parameter	Value
Major radius, R_0 (m)	3.1
Minor radius, a (m)	0.89
Aspect ratio, A	3.47
Plasma elongation, κ	1.70
Plasma triangularity, δ	0.40
Safety factor at 95% flux, q_{95}	3.0
TF at R_0, B_0 (T)	6.1
Plasma current, I_p (MA)	7.0
Normalized beta, β_N (%)	2.5
Confinement multiplier, H, ITER IPB98(y,2)	1.1
P_{fus} (MW)	150
$Q_p = P_{fus}/P_{aux}$	2
$\langle n_e \rangle$ (m^{-3})	2.0×10^{20}
$\langle n_e \rangle / n_{GW}$ (Greenwald density ratio)	0.75
$\langle T \rangle_n$ (keV)	7.6
Density profile exponent, α_n	0.1
Temperature profile exponent, α_T	1.0
Neutron wall load (MW/m^2)	0.79
First-wall power density (MW/m^2)	0.34
Total DT fusion neutron rate (number/s)	5.32×10^{19}
H-mode power flux margin, P_{sep}/P_{LH}^{thr}	4.5
Bootstrap current fraction	0.38

which satisfies the neutron source performance requirements, is within the allowable operating range.

The 7-MA/6.1-T design is also capable of higher performance operation with $Q_p = 5$, if higher levels of confinement or beta limits can be attained. In Fig. 6, a POPCON plot for an enhanced confinement factor $H = 1.3$ relative to the ITER IPB98(y,2) scaling is shown. It can be seen that operating points with higher Q_p's and fusion powers, and with densities below the Greenwald limit, are possible. It also should be emphasized that such confinement enhancements are rather modest and are routinely observed in today's experiments.[21]

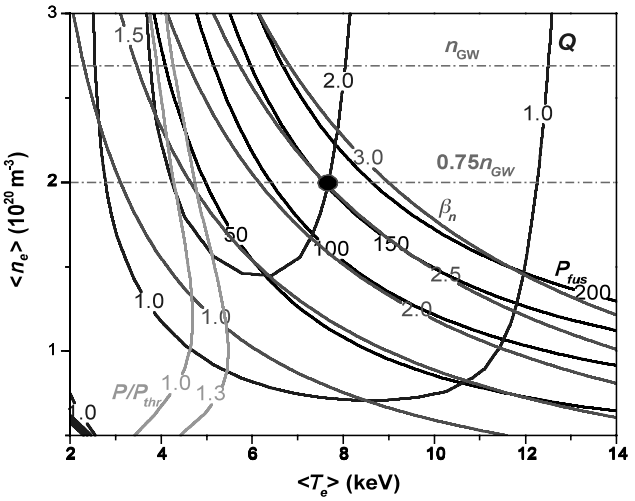

Fig. 5. POPCON plot for the reference design of the fusion neutron source. Contours of constant fusion power, Q_p, normalized beta and P_{sep}/P_{LH}^{thr} ratio are shown. In addition, lines of constant $\langle n_e \rangle / n_{GW}$ ratio are also shown. The reference operating point is marked by a solid circle.

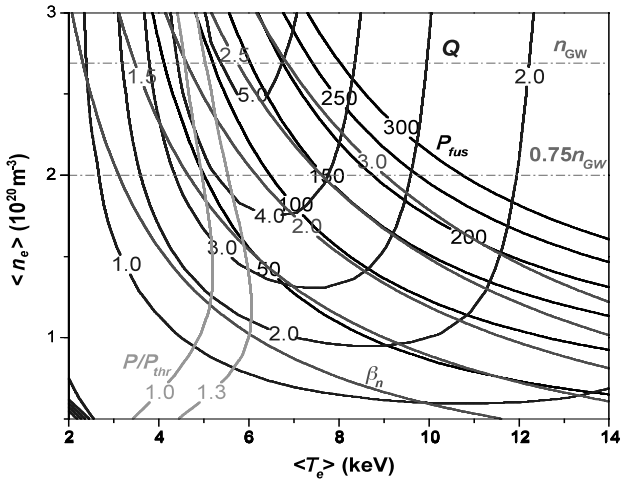

Fig. 6. POPCON plot assuming a confinement enhancement factor $H = 1.3$.

IV.B. Current Drive Considerations

Steady-state operation is one of the goals of the FTWR design. This means that external current drive will be required to supply part of the plasma current in the fusion reactor core. Since most current drive methods for reactor-grade plasmas are rather inefficient and expensive, every effort should be made to minimize the external current drive requirements by maximizing the bootstrap current fraction. For the reference design point, this fraction is estimated to be ~38% using a simple scaling formula (Appendix A). However, it is believed that higher bootstrap currents can be attained by optimizing various plasma profiles.

To get an idea of the influence of the bootstrap current fraction on the demands on the current drive system, the current drive efficiency $\eta_{CD} \equiv I_{CD}/P_{CD}$ (A/W) required for steady-state operation is calculated for our reference design for two values of the plasma Q_p. This calculation assumes that all of the auxiliary power injected into the plasma is also available to drive current; therefore, $I_p(1 - f_{bs}) = \eta_{CD} P_{fus}/Q_p$. The reference values for fusion power and plasma current (150 MW and 7 MA, respectively) have been assumed.

It can be seen from Table VI that for the reference design point, a current-drive efficiency in the range of

TABLE VI

Current Drive Efficiencies Required for Steady-State Operation for Various Bootstrap Fractions and Q_p Values

Bootstrap Current Fraction	η_{CD} (A/W), $Q_p = 2$	η_{CD} (A/W), $Q_p = 5$
0.2	0.075	0.187
0.4	0.056	0.140
0.6	0.037	0.093
0.8	0.019	0.047

0.05 to 0.06 A/W would be necessary to achieve steady-state operation. Although a detailed analysis of the current drive and heating system of this design has not been performed, a system based on fast waves (FW) in the ICRF regime for central current drive and lower hybrid (LH) waves for off-axis drive would be a reasonable choice.[22] An estimate of the FW current drive efficiency of such a system can be obtained by using a simple scaling formula developed for the ARIES RS design study.[22,23] For our reference design point, this simple scaling predicts a current drive efficiency of 0.03 A/W, resulting in a driven current of 2.34 MA, less than the 4.34 MA that is needed. However, this is a very conservative estimate. A fraction of the current would be driven by LH, which has a higher current drive efficiency than ICRF FW.

Furthermore, even if all the current had to be driven by FW current drive, we could operate at higher temperatures and lower densities to increase the current drive efficiency. As can be seen from the POPCON plot in Fig. 5, by moving along the 150-MW fusion power line (which almost coincides with the constant $\beta_N = 2.5$ contour) we can produce the same amount of fusion power at higher temperatures and lower densities. We would have to accept slightly lower Q_p operation, but this also works to our advantage in this case since the extra auxiliary power would be available to drive more current. A simple calculation shows that we could drive all of the 4.34-MA current needed for steady-state operation with FW current drive alone by operating at $Q_p \approx 1.55$ with $\langle T_e \rangle_n \approx 9$ keV and $\langle n_e \rangle \approx 1.6 \times 10^{20}$ m^{-3} to achieve a higher current drive efficiency ($\eta_{CD} = 0.044$ A/W).

Note also that intensive research is being carried out in the area of tokamak current drive, and the relevant experimental database is rapidly growing.[15] More efficient methods, such as electron cyclotron (EC) current drive, may soon be available.

IV.C. Extrapolations Beyond Present Experimental Database

Since the objective of this design is a relatively near-term neutron source to transmute spent nuclear fuel, one of our design requirements was to remain as close as possible to the present tokamak experimental database. However, even small extrapolations from this database can greatly enhance the performance and hence attractiveness of a fusion neutron source. Such extrapolations allow operation at a higher beta and enhanced confinement level (simultaneous attainment of higher beta and enhanced confinement is usually required) and result in higher fusion power densities and higher bootstrap current fractions. Tokamaks operating under these improved conditions are usually called advanced tokamaks, and are being vigorously studied by the fusion community.[21] Several tokamak experiments around the world have achieved advanced tokamak operation for short pulses, and this database is rapidly growing.

V. NEUTRON SOURCE TECHNOLOGY DESIGN

V.A. Magnets

A tokamak fusion neutron source requires several sets of magnets. A toroidal magnet system produces the toroidal magnetic field needed to stabilize the plasma, while a CS and a set of poloidal field (PF) ring coils provide the changing magnetic flux (volt-seconds) to drive the inductive plasma current and provide the equilibrium field for plasma position control and shaping.

In this initial analysis, we have focused our attention on the TF and CS systems, since they are the ones that affect the size of the FTWR and can have a major impact on the recirculating power fraction of the plant.

Our reference design is based on resistive copper magnets (with ceramic or organic insulators) cooled at cryogenic temperatures (80 to 100 K) by LN_2. This choice follows recent designs of pulsed tokamak plasma burning experiments, which have also adopted resistive magnets cooled at cryogenic temperatures, for simplicity and size reduction.[24–26]

A wedged design with 18 TF coils was adopted. One unique characteristic of the FTWR design is that the TF coils are larger than would be expected for a tokamak of this size, since there must be enough space between the plasma and outer TF coil leg to accommodate the transmutation reactor (see Fig. 1). Another unique feature is the requirement for steady state operation, which imposes rather demanding requirements on the LN_2 refrigeration system.

To minimize joule losses, OFHC copper was selected as the conductor material, with 3% steel added for structural support. Cooling channels occupy 5% of the TF coil cross section. To minimize the resistance of the coils while maintaining structural integrity, the cross sections of the top, bottom, and outer legs of the TF coils were 50% larger than the cross section of the inner leg.

To ensure that our TF coil design meets American Society of Mechanical Engineers (ASME) structural design criteria, the various stresses and forces (centering

TABLE VII

Major TF and CS Magnetic Coil Parameters

Parameter	TF Coils	CS Coil
Conductor	OFHC Cu	OFHC Cu
Coolant	LN_2	LN_2
Field at conductor (T)	10.45	8.0
Cross section area (m^2)	0.22	0.547
Coolant fraction (%)	5	5
Steel fraction (%)	3	20
Maximum tensile stress (MPa)	132	246
ASME allowable Sm (MPa)	132	251
Ohmic heating (MW)	82 (all magnets)	27
Magnet resistance (Ω)	1.645×10^{-7} (per magnet)	7.133×10^{-8}

and tensile forces, bending stresses, etc.) were evaluated using standard analytic expressions (Appendix C). The yield and ultimate strengths for the magnet materials are listed in Appendix B.

The CS coil was designed to produce ~45 V·s, which, along with the contribution from the PF coil system (assumed to be equal to the CS contribution), is sufficient to start up the plasma and provide enough volt-seconds for a few minutes of burn (flattop) time. The same materials (OFHC and steel) were used for the CS coil, but the steel fraction was higher (20%) compared to the TF coil design. Twenty-five coolant channels (5% of the cross-sectional area of the CS coil) were used.

The major design and operational parameters of the TF and CS coil systems are summarized in Table VII.

Radiation effects on the magnets, particularly the insulators, are a concern for the FTWR design. Transport calculations indicate that the lifetime fast neutron fluence at the TF coil of 1.8×10^{22} n/cm^2 is a factor of ~2 less than the limiting value for ceramic insulators but that the lifetime dose of 1.5×10^{12} rads exceeds the limit for organic insulators. Although the radiation damage limits for insulators are uncertain, the values used here are comparable to those used in other design studies.[27–29]

V.B. Heat Removal from Magnets

Joule heating and heat removal calculations have been made using standard analytical expressions. The use of LN_2-cooled resistive magnets has helped to drop the joule heating losses from the TF and CS coils to 109 MW. This is more than an order of magnitude less than the amount of heat that would have to be removed (~1.3 GW) had we selected water-cooled magnets. The power required to operate the LN_2 refrigeration cycle is, however, considerable. We estimate that 7 W of electricity is needed for each watt of heat that must be removed.[30] Therefore, the total amount of electric power required to operate and cool the TF and CS coils is 872 MW. Although we have not designed the PF coil system, there is no comparable constraint on the cross section area that can be used to reduce resistance, and we allow 100 MW(electric) for dissipation and LN_2 refrigeration in the PF coils. The total, 972 MW(electric), is a significant fraction of the total recirculating power of the plant, but it is still smaller than the amount that would be needed with water as the coolant.

V.C. First Wall

The first wall is the material surface closest to the plasma and, along with the divertor plates, absorbs the radiation and charged particle energy escaping from the plasma. It is necessary to ensure that the first-wall material can withstand the various thermal and coolant stresses (i.e., satisfy the ASME structural criteria) and that the coolant can remove the heat that is deposited in the first wall. Some constraints on the FTWR design are the need for compatibility between the first wall and the transmutation reactor coolants and the need to minimize neutron absorption in the first wall.

A steel similar to HT-9 was selected as the first-wall material, since there is considerable experience with this material in the nuclear field[31]; it is being developed in the fusion program, and it has been investigated as a first-wall material in several fusion reactor studies.[32–35]

The same lead-lithium coolant used in the transmutation reactor was chosen as the first-wall coolant. Although liquid metals have a significantly lower heat capacity than water, their selection as a first-wall coolant avoids any potentially adverse reactions between water and the transmutation reactor's lead-lithium coolant. In addition, since pressurization is not required, a thinner first wall is possible, which is important from the neutron economy point of view.

The basic first-wall design configuration was adapted from the ITER design.[16] A two-loop design was adopted (i.e., there are two independent coolant loops, one on the inboard and one on the outboard sides). The plasma-facing surface is coated with a 0.5-cm layer of beryllium, and the structural part of the first wall consists of a 2-cm thickness of HT-9-like steel, with 9-mm-diam coolant channels spaced at a distance of 2 cm.

The first wall was designed for a heat flux of 0.5 MW/m^2, higher than the reference value of 0.34 MW/m^2, to provide some margin for peaking, unexpected transients, and possible lower Q_p or higher fusion power operation. For the design heat flux, 38.25 MW of power will have to be removed from each of the two coolant loops. There are 700 coolant channels in the inner part and 1260 in the outer. A flow velocity of 1.13 m/s is

required for inlet and outlet coolant temperatures of 548 and 848 K, respectively.

Although the radiation damage limit for HT-9-type ferritic steels is not yet known, estimates in the range 100 to 200 dpa have been used[32–35] for fusion neutron spectra. The 623-day reference fuel cycle for the FTWR produces 21 dpa in the first wall. Thus, using the lifetime range 100 to 200 dpa, we estimate the first wall will have a lifetime of 5 to 10 fuel cycles. The plant design lifetime of 40 FPY is slightly more than 23 fuel cycles. This means that the first wall will have to be replaced (during a refueling shutdown) about 2 to 4 times over the plant lifetime.

VI. TRANSMUTATION REACTOR DESIGN

VI.A. Materials and Geometry

The transmutation reactor consists of the following materials. The fuel is a transuranic zirconium alloy (TRU-10Zr) dispersed in a zirconium matrix and clad with a steel similar to HT-9. The relative amounts of actinides and zirconium in the fuel region are adjusted to achieve the desired neutron multiplication (k_{eff} = 0.95) at the beginning of each cycle. At equilibrium, the actinides will constitute approximately 45% of the fuel volume. The coolant and tritium breeding material is the eutectic Li17Pb83. Properties of these materials are given in Appendix B.

The geometric configuration of the FTWR is shown in Fig. 1. The blanket is the region inside of the TF coils and outside of the plasma chamber. The blanket consists of the transmutation reactor, reflector, shield, first wall, and vacuum vessel. The transmutation reactor region, where the actinide-containing fuel assemblies are located, is outboard of the plasma and inside the TF coils. The design of the FTWR transmutation reactor is based on the ANL ATW blanket design studies.[17,36] The same pin and assembly geometry was used, with the exception that the length of the assembly was increased to 228 cm. Table VIII gives the basic data for the fuel assembly design.

The assemblies will be placed on the outboard side of the plasma chamber as shown Fig. 7. The reactor region is ~40 cm thick and will consist of 470 assemblies, of which $\sim\frac{1}{5}$ will be configured as "half assemblies" placed in the gaps along the interior and exterior surfaces of the reactor region to produce a more uniform annular distribution.

VI.B. Nuclear Design

The nuclear analysis was performed with the same codes and similar methodology used in the ANL ATW design studies.[17,36] The fuel cycle analysis was performed with the REBUS fuel cycle code.[37] Within this code, the neutronics calculations were performed using the DANT code[38] to perform two-dimensional discrete ordinates transport calculations with material-dependent multigroup cross-section libraries based on the ENDF/B-V.2 nuclear data library processed using the MC^2-2 (Ref. 39) and SDX (Ref. 40) codes for a 34-group energy structure. The REBUS input specifies the compositions, geometries, and all other necessary fuel cycle parameters. The neutronics calculations were performed using an *R*-*Z* geometry model, with *R* in the direction of the major radius.

TABLE VIII

Fuel Assembly Design

Pin diameter (cm)	0.635
Clad thickness (cm)	0.05588
Pitch	Triangular
Pitch to diameter	1.727
Pins per assembly	217
Structure pins	7
Fuel smear density	85%
Hexagonal assembly pitch	16.1
Assembly length (cm)	228
Assemblies	470
Average power density (kW/ℓ)	124
Volume%	
Fuel	17.01
Structure	10.44
Coolant	69.55
Materials	
Fuel	TRU-10Zr/Zr
Structure	HT-9
Coolant	Li17Pb83

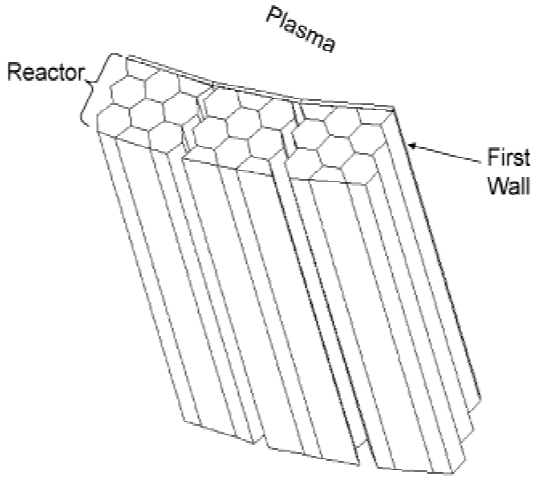

Fig. 7. Transmutation reactor configuration outboard of plasma chamber.

TABLE IX

Nuclear Design Requirements

Requirement	Limit
Criticality safety	$k_{eff} \leq 0.95$
Tritium self-sufficient	Tritium inventory ≥ required startup inventory
Fuel integrity	Fuel cladding irradiation <200 dpa (Ref. 41)
First-wall integrity	First-wall irradiation <200 dpa (Ref. 41)
Neutron source strength	$P_{fus} \leq 150$ MW
Fuel material composition	≤45% actinides by volume (Ref. 17)
Heat removal	$P_{blanket} \approx 3000$ MW
Plant life	40 FPY
Plant availability	60%

TABLE X

Fuel Cycle Performance Summary

Cycle length (FPDs)	623
Enrichment (volume fraction TRU)	47%
BOC neutron multiplication	0.950
EOC neutron multiplication	0.852
Fuel batches	4
Actinide loading (MT)	27
Discharge burnup (4 cycles)	25%
First-wall irradiation rate (dpa/cycle)	21
Cladding irradiation (dpa/4 cycles)	150
SNF waste transmutation (MTU/FPY)	102

The blanket power consists of the fission power, the energy deposited by the 14.1-MeV fusion neutrons, and all of the exoergic reactions such as $^6\mathrm{Li}(n,T)$. The total power includes the 3000 MW of blanket power, the alpha fraction ($\frac{1}{5}$) of the fusion power, and the auxiliary heating power of the plasma. Under this operating scheme, the fission power, fusion power, and total power will vary over the cycle. In the reference cycle, the total system power will rise from 3029 MW at beginning of cycle (BOC) to 3093 MW at the end of cycle (EOC).

The nuclear design requirements are shown in Table IX. The neutron multiplication at the beginning of each cycle was limited to $k_{eff} = 0.95$, to provide a large margin against accidental criticality. To achieve this value of k_{eff}, the fuel enrichment is adjusted. Compensation for reactivity decrease with burnup could be accomplished in a number of ways. We have chosen to proceed with a simple operational scheme in which the fusion neutron source strength will increase over the cycle to maintain a constant power of 3000 MW in the transmutation reactor. The fusion power will rise from 41 MW at BOC to 133 MW at EOC. Reactivity loss from fuel burnup is not compensated by any type of reactivity adjustment.

The fusion power limit of 150 MW determines the maximum reactivity swing over a cycle. Radiation damage of the fuel cladding limits the achievable burnup in a fuel element. To maximize the cumulative burnup while limiting the reactivity swing, a batch fueling scheme was adopted. The assemblies will be loaded with four batches of fuel in a roughly out-to-in pattern, with the "fresh" SNF fuel being loaded farthest from the plasma and the highest burned fuel closest to the plasma neutron source.

The nuclear performance is summarized in Table X. The reference fuel cycle length is 623 full power days (FPDs). A discharge burnup of 25% of the actinides will be achieved during the fuel in-reactor residence of four 623-FPD cycles. The actinide fission rate is 1.13 metric tonnes (MT) per FPY. Over the 40-FPY lifetime, the transuranic inventory recycled from ~4,500 MTU of spent LWR fuel will be fissioned in a single FTWR.

VI.C. Heat Removal and Pumping Power

We have divided the blanket into four large regions to estimate the pumping power required to remove the heat. These regions are the reactor, reflector, shield, and first wall. The requirements of the first wall were discussed in Sec. V. The majority of the energy will be from fission in the reactor region, with much smaller amounts deposited in the other regions. The inlet temperature in each region is the same, and the flow velocity through each region is adjusted so that the outlet temperatures are also the same. Following the ARIES-I design report,[42] the inlet and outlet temperatures are set at 548 and 848 K, respectively. The resulting flow velocity is 0.76 m/s in the reactor region. The total coolant mass flow rate for the entire blanket is 53 MT/s.

The pumping power requirement has three separate components: the conventional friction losses, the potential energy gains, and the MHD losses. The density of the heavy Li17Pb83 coolant causes the power required to lift the fluid to be significant. We assume that the resulting potential energy increase will be lost in the heat exchanger. The pumping power calculation is described in Appendix D. Each region has three flow paths that need to be included. The first is the path for moving the coolant horizontally from outside the TF coils into the region of interest, the second is the flow path for moving it vertically through the region of interest, and the last is the flow path for moving it horizontally back outside the TF coils.

Table XI summarizes the pumping power calculations. The total pumping power, based on a 90% pumping efficiency,[34] is 130 MW, of which 123 MW is from MHD losses. If an electrical insulator were to be developed to coat the piping and fuel cladding, the MHD pumping loss could be reduced to effectively zero.

TABLE XI

Blanket Pumping Power

Parameter	Reactor	Reflector	Shield
Radius from centerline (m)	4.25	3.75	3.61
Flow length through region (m)	2.28	2.38	2.48
Magnetic field in region (T)	4.25	4.82	5.00
Flow length to/from region (m)	0.90	1.47	1.60
Magnetic field to/from region (T)	3.84	4.03	4.09
Region power (MW)	2922	28	63
Peaking factor	1.50	2.05	7.33
Mass flow rate (kg/s)	51630	491	1115
Flow velocity (m/s)	0.76	0.04	0.08
MHD pumping through region (MW)	74	0.0	0.2
MHD pumping power to/from region (MW)	48	0.04	0.18
Friction pumping power (MW)	6.7	0.00	0.00
Gravity pumping power (MW)	1.1	0.01	0.02
Total pumping power (MW)	130	0.09	0.42

VI.D. Tritium Breeding

The requirement to produce tritium from neutron capture in lithium has a significant impact on the overall design. We have chosen to include lithium in a liquid form as part of the Li17Pb83 to allow continuous recovery of the tritium. The FTWR is designed to be tritium self-sufficient; i.e., although the initial tritium inventory required to start up the reactor will be acquired externally, no additional tritium will be required from external sources for the life of the plant. The tritium inventory calculation procedure is described in Appendix E.

The BOC inventory is a function of the fusion rate and the operating parameters of the tritium system. We used a simple estimate of the BOC tritium inventory—a tritium inventory equivalent to the total number of fusions occurring in the first 30 FPDs of operation must be available at the beginning of each cycle. The BOC tritium inventory for the reference fuel cycle is 120 g. The cycle length is not very sensitive to this parameter. A larger inventory requires slightly higher tritium production to offset the higher radioactive decay rate, which is very small relative to the fusion rate.

The fusion power, hence the tritium consumption rate, will increase by nearly a factor of 4 over a cycle. The tritium production rate will also increase somewhat because of changes in the spectrum due to a higher fraction of 14.1-MeV neutrons. Over a cycle, the tritium production will initially be larger than the fusion rate, and the inventory will grow until the tritium consumption rate equals the tritium production rate and then fall rapidly as the tritium is burned at an increasing rate. The peak tritium inventory for the reference cycle in the FTWR is $\approx$1000 g. The cycle length is limited to the time at which there would be just enough tritium to satisfy the startup requirements for the next cycle, allowing for a conservative 90 days of decay between cycles, which requires an EOC tritium inventory of 121g. To achieve this, the lithium must be enriched to 20% ^{6}Li.

The threshold for tritium production in ^{7}Li is 2.82 MeV, well below the energy of most fission neutrons. In this design, the neutron spectrum is predominately in the region of the minima of the natural lithium cross section, below the threshold of ^{7}Li and above the epithermal resonance of ^{6}Li. We have not attempted to exploit the larger cross sections of ^{6}Li at lower energies, but if tritium production needs to be increased, the addition of graphite or other moderators in the reflector and/or shield should allow for large increases in the tritium production by shifting the spectrum down into the ^{6}Li resonance.

VII. REFLECTOR AND SHIELD DESIGN

The purpose of the shield is to protect the magnets from radiation damage, and the purpose of the reflector is to redirect escaping neutrons back into the transmutation reactor. The shield-reflector is located just in front of the TF magnets between the magnets and the sources of neutrons from the plasma and the transmutation reactor, and on the top and bottom of the plasma and the transmutation reactor (see Figs. 1 and 2). We used the compositions of the reflector and shield from the ANL ATW design studies[17,36] shown in Table XII.

The magnets are designed as lifetime components. Radiation damage limits to magnet insulators of 10^{11} rads for organic insulators and 4×10^{22} fast neutrons per cm^2 for the inorganic insulators[27] were used as design criteria. Transport calculations determined that the

TABLE XII

Reflector and Shield Composition

Region	Structure (HT-9)	Coolant (Li17Pb83)	Boron Carbide (B_4C)
Reflector	70%	30%	
Shield	25%	18%	45%

maximum radiation doses in the TF magnets would be 1.5×10^{12} rads and 1.8×10^{22} n/cm^2, which implies that the present shield design would allow the use of ceramic insulators but not organic insulators. However, the insulator radiation damage limits are rather uncertain, and it is possible to choose more effective shield materials.

The minimum thickness of the inboard reflector plus shield plus vacuum vessel plus first wall is ~30 cm. The reflector and shield are 8.5 and 17 cm thick, respectively. Varying the composition of the reflector/shield ratio showed that this is about the minimum. The same thicknesses are used above and below the plasma and the transmutation reactor and outboard the reactor.

The total thickness inboard of the plasma is 40 cm. This includes 30 cm for the reflector, shield, first wall, and vacuum vessel, plus a 10 cm gap to accommodate the assembly of the components.

VIII. TRANSMUTATION FUEL CYCLE ANALYSIS

VIII.A. LWR Waste/Transmutation Reactor Feed Composition

The SNF that will be transmuted by the FTWR will ultimately come from a very large number of LWRs that have been and will be operated under a wide range of operating conditions with varying fuel design, discharge burnups, and storage times. This will result in significant variance in the feed composition to the FTWR. For the reference fuel cycle analysis, we use a single feed composition that is representative of the material we would expect to receive. The composition is based on removal of 99.995% of the uranium[43] from the remaining actinides. Since many of the minor components are important to some of the parameters we are evaluating, a complete isotopic composition is needed. This was not available, so the depletion of a pressurized water reactor (PWR) pin cell was performed using SCALE 4.4 (Ref. 44). A design and burnup calculation that gives reasonably good agreement with Ref. 43 for the major isotopes was performed. This should be representative of the composition of the minor isotopes and fission products that will be present. Table XIII shows the reference composition compared with that used by ANL for its design studies[43] and with the average composition from the Yucca Mountain Environmental Impact Statement.[45] The differences all tend to be fairly small and should not have a significant impact on the reference fuel cycle calculations.

TABLE XIII

Transmuter Feed Actinide Composition

Isotope	Design Composition	Absolute Difference with ANL (Ref. 43)	Absolute Difference with YMEIS (Ref. 45)
^{235}U	0.0039%	0.00%	0.00%
^{236}U	0.0018%	0.00%	0.00%
^{238}U	0.4234%	−0.05%	0.00%
^{237}Np	4.3128%	−0.71%	−1.29%
^{239}Pu	53.9014%	0.71%	1.73%
^{240}Pu	21.2309%	−0.30%	0.15%
^{241}Pu	3.8702%	0.09%	0.33%
^{242}Pu	4.6769%	−0.01%	0.05%
^{241}Am	9.1838%	0.22%	−0.25%
^{242m}Am	0.0067%	−0.01%	−0.01%
^{243}Am	1.0205%	0.09%	−0.18%
^{243}Cm	0.0018%	0.00%	0.00%
^{244}Cm	0.1158%	0.01%	−0.04%
^{245}Cm	0.0125%	0.00%	−0.01%
^{246}Cm	0.0010%	0.00%	0.00%

VIII.B. Waste Processing

The waste processing system for the FTWR will be identical to the waste processing system being developed for the ATW system.[46] The general concept of this system is shown in Fig. 8. The waste processing system consists of three basic components. The first is a URanium EXtraction system (UREX) that will separate the bulk uranium and fission products in the SNF from the transuranic elements. The transuranic elements and the rare earth fission products will then be transferred to a pyrometallurgical system (Pyro-A) that will separate the rare earths from the transuranic elements and convert the latter to a metallic form for fuel manufacturing. The

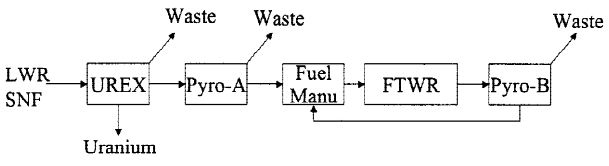

Fig. 8. Waste processing flow diagram.

discharged FTWR fuel will be sent to a separate pyrometallurgical system (Pyro-B) where the residual actinides will be recovered. The recovered materials from Pyro-A and Pyro-B will be blended together and manufactured into new fuel elements for the FTWR.

Many of the performance parameters are very sensitive to the performance of the waste processing systems. The UREX system is assumed to remove 99.995% of the uranium[43] and all of the fission products that are not rare earth elements. The Pyro-A system is assumed to remove 95% of the rare earth fission products[17] and recover 99.9% of the actinide elements. The Pyro-B system is assumed to remove 95% of the rare earth fission products, remove 100% of all other fission products, and recover 99.9% of the actinide elements. In addition to the recovery fractions, the total fraction of transuranics that end up in the waste stream is a strong function of fractional burnup achieved during each residence in the FTWR. The following equation shows this relationship:

$$f_{waste} = f_{\mathrm{UREX}}^{\mathrm{TRU}} + (1 - f_{\mathrm{UREX}}^{\mathrm{TRU}} + M_{\mathrm{SNF}}^{\mathrm{U}}(1 - f_{\mathrm{UREX}}^{\mathrm{U}})) \times \left(f_{\text{Pyro-A}} + \frac{(1 - f_{\text{Pyro-A}})(1 - f_{BU}) f_{\text{Pyro-B}}}{1 - (1 - f_{BU})(1 - f_{\text{Pyro-B}})} \right) , \quad (3)$$

where

$f_{\mathrm{UREX}}^{\mathrm{TRU}}$ = fraction of transuranics lost in UREX process = 0

$f_{\mathrm{UREX}}^{\mathrm{U}}$ = fraction of uranium recovered in UREX process = 99.995%

$M_{\mathrm{SNF}}^{\mathrm{U}}$ = relative mass of uranium in LWR SNF = 95

$f_{\text{Pyro-A}}$ = fraction of actinides lost in Pyro-A process = 0.1%

$f_{\text{Pyro-B}}$ = fraction of actinides lost in Pyro-B process = 0.1%

f_{BU} = fractional burnup of actinides in a single residence in the FTWR.

This relationship includes the uranium that is not recovered in the UREX process as transuranics, since most of this will be converted to transuranics in the FTWR. For the FTWR, each MTU of SNF will result in 70 g of transuranics in the waste stream. This is a 99.4% destruction of the transuranics originally present in the SNF.

VIII.C. Equilibrium Cycle Calculations

The equilibrium fuel cycle calculation procedure is described in Appendix F. Initially, the first generation of FTWRs will only have feed from LWR SNF. The pyrometallurgical technology allows for a very short decay period of the SNF before recycling. The reference fuel cycle assumes that the FTWR fuel will remain in the reactor for four cycles and then be reprocessed, blended with fresh SNF, and fabricated into new fuel elements for reinsertion into an FTWR. Over the 40-FPY plant life of the first generation of FTWRs, the original charge of LWR feed will be reprocessed five times.

This implies that fuel composition in the first generation FTWRs will be very near equilibrium well before the end of life. The earlier cycles can be loaded to perform similarly to the equilibrium cycle. The initial charge of the reactor and the first reload batch will require ~3500 MTU of LWR SNF to manufacture these fuel elements. Following this, ~190 MTU of LWR SNF will be processed in each subsequent 623-day cycle. A first generation FTWR will process ~74 MT of transuranics from LWR SNF of which ~56% will be fissioned, 0.2% will be lost to the waste streams, and 44% will be used in a second-generation FTWR.

The second and subsequent generations of FTWRs will use the fuel from the previous generation FTWRs and therefore operate in the equilibrium mode over their entire lives. Repeated recycling of the discharged transuranics from FTWRs in successive generations of FTWRs will ultimately result in the destruction of 99.4% of the transuranics discharged from LWRs operating on the OTC.

The change in composition is summarized in Table XIV. All values are the mass fraction of the total actinide inventory. Table XIV shows that even in this very hard neutron spectrum, there is a significant shift to the higher elements. The curium concentration increases by nearly a factor of 10. The increase in the uranium concentration results from the buildup of ^{234}U. A high concentration of ^{238}Pu builds up in the reactor from absorption in ^{237}Np and alpha decay of ^{242}Cm. The ^{238}Pu decays to ^{234}U with a half-life of 87.7 yr. Plutonium will still constitute the majority of the mass of actinides in the reference fuel cycle, but the isotopic composition will change dramatically. The ^{239}Pu fraction drops from

TABLE XIV

Change in FTWR Actinide Composition over the Four 623-Day Cycles Between Reprocessing

Element	SNF Feed	FTWR Charged	FTWR Discharge
Mass (MT)	1.93	7.87	5.88
U	0.4%	4.0%	5.1%
Np	4.3%	3.5%	3.2%
^{238}Pu	1.2%	4.8%	5.9%
^{239}Pu	53.9%	31.0%	23.1%
^{240}Pu	21.2%	30.6%	33.8%
^{241}Pu	3.9%	3.1%	3.3%
^{242}Pu	4.7%	9.1%	10.7%
Am	10.2%	12.9	13.5%
Cm	0.1%	1.0%	1.5%

54% of the mass of all actinides and 63% of the plutonium mass in the LWR SNF feed to 23% of the actinide mass and 30% of the plutonium mass in the fuel discharged from the reference FTWR cycle.

VIII.D. Transmutation Performance Characteristics

The FTWR is essentially a hazardous waste incinerator. Its primary goal is to take a hazardous material and convert it to less hazardous materials that are easier to dispose of in a manner that is cheaper than the alternative of directly disposing of the original SNF. The FTWR would not eliminate the need for a high-level waste repository, but it would greatly reduce the performance that must be achieved by the repository to protect the public.

The hazardous waste incinerator will charge a fee for taking the waste, perhaps generate revenue by selling its net electrical production, and be assessed a fee for disposing of its own, hopefully, less hazardous waste.

This initial analysis is not sophisticated enough to evaluate the cost or to do a thorough assessment of the relative hazard of the OTC versus the FTWR cycle. Therefore, we evaluate surrogate figures of merit to provide indications of performance of the FTWR as a hazardous waste incinerator. We examine two parameters: mass flow and toxicity flow.

The mass flows of the various elements and of a few specific isotopes are given in Table XIV. For the OTC, ~11 000 g of transuranics will be placed directly in a repository for each metric tonne of initial uranium content (MTU) of LWR fuel discharged. When the same SNF discharged from an LWR is reprocessed and cycled through the FTWR transmutation cycle, ~70 g of transuranics per MTU will end up in the repository. This is a 99.4% reduction in the mass of the transuranics that ultimately end up in the repository.

The toxicity flow is often evaluated for transmutation systems. Figure 9 shows the flow diagram for the FTWR cycle. The toxicity is defined as the cubic metres of water required to dilute the given material to the radioactive concentration guides for continuous ingestion from water. The toxicity was calculated using the water dilution factors included in SCALE 4.4 (Ref. 44).

The toxicity is strongly time dependent. Initially, the toxicity is dominated by the highly radioactive, but short-lived, fission product isotopes. As the short-lived isotopes decay away, the medium-lived actinides and fission products become important. At very long decay times, the daughter products of the very long-lived isotopes, such as ^{238}U, will dominate the toxicity. To put these numbers in context, the toxicity flow for the entire nuclear fuel cycle (as depicted in Fig. 9) is given in Table XV. Table XV includes the toxicity as a function of time for each stage of the fuel cycle and for the separate components produced at each stage. For example, line 1 gives the toxicity of uranium ore as it exists in nature, while lines 2 and 3 give the toxicity of the two components of uranium ore—natural uranium and the mill tails.

There are two waste system summaries for the OTC and FTWR scenarios. The first (lines 14 and 15) treats the uranium streams as part of the total waste stream, and the second (lines 16 and 17) includes only the wastes that must end up in a high-level waste repository. The repository waste for the OTC is the LWR SNF shown in the sixth row of Table XV. For the FTWR, all fission products and actinides that are not recovered and recycled back into the FTWR are assumed to go to a repository, as indicated in lines 8 and 13.

Initially, the waste from the FTWR fuel cycle has a greater toxicity than that of the OTC, because of the creation of additional fission products and short-lived actinides in the SNF that is recycled in the FTWR. In the 100- to 500-yr time period, the toxicity of the FTWR waste falls below that of the OTC. At very long times, the radiotoxicity of the ^{238}U daughters in the depleted uranium dominates the toxicity, and only a small reduction in radiotoxicity is produced by the FTWR fuel cycle compared to the OTC, when the uranium is considered as part of the waste stream.

However, the uranium can be separated from the high-level waste stream and stored in a low-level waste facility. If only the repository requirements for high-level wastes are considered (the case depicted in the last two lines of Table XV and in Fig. 3), the toxicity of the FTWR fuel cycle waste will fall well below that of

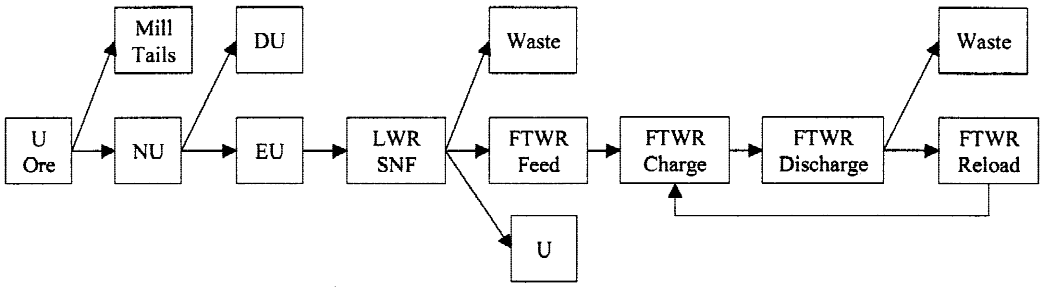

Fig. 9. FTWR toxicity flow diagram.

TABLE XV

Fuel Cycle Toxicity Flow for 1 Metric Tonne of Enriched Uranium in Original LWR Fuel*

Source	Component	Mass (MT)	Toxicity (m^3 of H_2O) at Time (yr)						
			0	100	500	1000	10 000	100 000	1 000 000
U Ore	U Ore	7.700	1.2E+08[a]	1.2E+08	1.2E+08	1.2E+08	1.2E+08	1.2E+08	1.2E+08
U Ore	Tails	0.000	1.2E+08	1.2E+08	1.2E+08	1.2E+08	1.1E+08	4.8E+07	1.2E+04
	NU	7.700	1.5E+05	2.9E+05	3.9E+05	5.8E+05	9.1E+06	7.5E+07	1.2E+08
NU	DU	6.700	7.4E+04	1.8E+05	2.1E+05	2.5E+05	2.3E+06	2.4E+07	9.2E+07
	EU	1.000	8.0E+04	1.1E+05	1.8E+05	3.3E+05	6.8E+06	5.2E+07	2.9E+07
EU	LWR SNF	1.000	4.6E+11	2.4E+10	7.6E+08	4.3E+08	1.1E+08	6.8E+07	3.0E+07
LWR SNF	Recovered U	0.955	7.1E+04	9.4E+04	1.3E+05	2.3E+05	5.1E+06	4.0E+07	2.0E+07
	Waste	0.033	4.5E+11	2.2E+10	2.9E+06	1.3E+06	9.8E+05	7.8E+05	5.6E+05
	FTWR feed	0.011	8.0E+09	1.5E+09	7.6E+08	4.3E+08	1.0E+08	2.7E+07	9.1E+06
FTWR	Charge	0.046	3.3E+12	9.1E+09	3.4E+09	1.8E+09	4.6E+08	4.8E+08	9.8E+07
	Discharge	0.046	2.8E+13	1.0E+10	2.6E+09	1.4E+09	3.6E+08	4.6E+08	8.8E+07
FTWR discharge	Reload	0.034	1.4E+12	7.7E+09	2.6E+09	1.4E+09	3.6E+08	4.6E+08	8.8E+07
	Waste	0.012	2.7E+13	2.8E+09	3.1E+06	1.7E+06	6.7E+05	7.2E+05	2.7E+05
All waste streams	OTC waste	7.700	4.6E+11	2.4E+10	8.8E+08	5.5E+08	2.2E+08	1.4E+08	1.2E+08
	FTWR waste	7.700	2.7E+13	2.5E+10	1.3E+08	1.2E+08	1.2E+08	1.1E+08	1.1E+08
High level waste	OTC waste	1.000	4.6E+11	2.4E+10	7.6E+08	4.3E+08	1.1E+08	6.8E+07	3.0E+07
	FTWR waste	0.045	2.7E+13	2.5E+10	6.0E+06	3.0E+06	1.7E+06	1.5E+06	8.3E+05

*NU = natural uranium; EU = enriched uranium; DU = depleted uranium.
[a]Read as 1.2×10^8

as-mined uranium ore in ~500 yr. The toxicity of the high-level waste in the SNF from the OTC, on the other hand, requires ~7500 yr to be reduced to this level of toxicity. There are other hazard metrics that would dictate longer periods of storage, but this comparison is indicative of the reduction in hazard potential that can be achieved by recycling SNF in FTWRs.

VIII.E. System Deployment

According to the U.S. Department of Energy Integrated Data Base Report,[47] the U.S. inventory of discharged LWR SNF was 34 252 MTU in 1996. The inventory is expected to grow at a rate of slightly over 2000 MTU/yr for >10 yr. There are a number of scenarios for the total inventory of SNF that will be discharged after that. A realistic estimate is that the present nuclear capacity will be maintained into the foreseeable future, in which case the feed into the inventory will be slightly >2000 MTU/yr. If the nuclear capacity is increased or decreased, then the feed into the SNF inventory will increase or decrease accordingly.

We assessed a simple scenario for the deployment of a fleet of FTWRs to give a sense of the magnitude and time frame that would be needed to destroy the backlog of LWR SNF and to support a fleet of LWRs at equilibrium conditions in the future. This assessment is based on the assumption of a constant electrical power generation of 100 GW(electric) from LWRs. This scenario assumes that the first FTWR demonstration facility is deployed in 2020 and operates for 10 yr before we enter the slow growth phase. During the slow growth phase, a single FTWR is added each year for the next 10 yr. This phase is followed by the fast growth phase, during which two FTWRs are added every year. The fast growth phase would last for >20 yr. This phase is followed by the equilibrium phase, during which FTWRs are added at a rate just sufficient to maintain the equilibrium FTWR fleet. The key parameters are given in Table XVI. At equilibrium, each 3.0-GW(thermal) FTWR would support 3.0 GW(electric) of LWRs.

The cost of an FTWR would be greater than the cost of an LWR, and the multiple processing costs involved in the fuel cycle of an FTWR would probably be greater than the cost of producing fresh fuel for an LWR. On the other hand, the costs of building additional repositories for long-term storage of LWR SNF would be decreased substantially by using the FTWR. A quantitative

TABLE XVI

FTWR Fleet Deployment Parameters

Installed LWR capacity [GW(electric)]	100
LWR capacity factor	80%
LWR thermal efficiency	35%
Average LWR burnup (GWd/MTU)	40
LWR TRU concentration in future discharges	1.1%
LWR TRU inventory feed rate (MTU/yr)	2 087
LWR SNF inventory (MTU) in 2000	42 600
TRU concentration in SNF in 2000	1.0%
FTWR fission capacity (MT/FPY)	1.14
FTWR availability	60%
Support ratio [GW(electric) LWR/FTWR]	3.0
Steady state number of 3000-MW(thermal) FTWRs	34

cost analysis is necessary, but beyond the scope of this paper.

Figure 10 shows the inventory of transuranic waste as a function of time for the above scenario, for different assumptions about the availability of the FTWR. The higher the availability in the slow growth and fast growth phases defined above, the earlier in time the maximum inventory occurs and the lower are both the maximum and equilibrium inventories. With the reference availability (60%), the transuranic inventory would begin to decline after 2050 and would approach equilibrium by approximately 2120.

IX. ELECTRIC POWER PERFORMANCE ANALYSIS

A design objective of the FTWR is electric power self-sufficiency. The level of self-sufficiency of the design is characterized by the electric power amplification factor, also known as the engineering "Q" of the reactor, which is just the inverse of the recirculating power fraction, being at least unity:

$$Q_e = \frac{\text{gross electric power produced}}{\text{gross electric power consumed}} \geq 1 \ . \qquad (4)$$

The gross electric power produced, P_{EG}, is given by

$$P_{EG} = \eta_{th}\left[P_{fus}\left(\frac{1}{5} + \frac{1}{Q_p}\right) + P_{reac}\right] , \qquad (5)$$

where the first term represents the power deposited on the plasma-facing components (mainly charged particles and radiation) and P_{reac} represents the total power (including the fusion neutron contribution) deposited in the transmutation reactor region (predominantly fission power).

The total electric power consumed by the power plant to operate its various components P_{plant} is then given by

$$P_{plant} = \frac{P_{fus}}{\eta^e_{\rm CD} Q_p} + P^{\rm TF}_{tot} + P^{\rm CS}_{tot} + P^{\rm PF}_{tot} + P_{p\text{-FW}} + P_{p\text{-}reac} + P_{repro} + P_{BOP} + P_{other} \ , \qquad (6)$$

where

$\eta^e_{\rm CD}$ = wall-to-plasma electric efficiency of the current drive and heating system

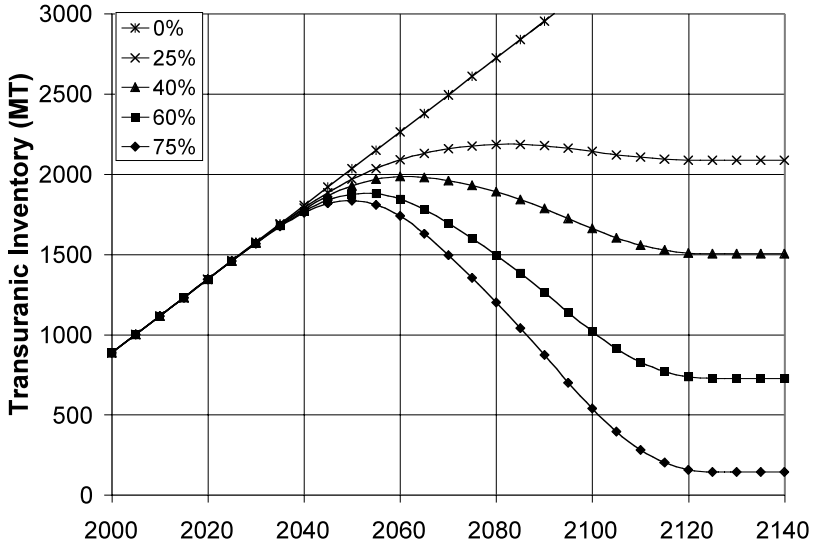

Fig. 10. Estimated future transuranic inventory as a function of FTWR availability (0% corresponds to the OTC without FTWRs).

P_{tot}^{TF} = total (I^2R joule heating term plus refrigeration) electric powers required to operate the TF magnetic coil system

P_{tot}^{CS} = total (I^2R joule heating term plus refrigeration) electric power required to operate the CS magnetic coil system

P_{tot}^{PF} = total (I^2R joule heating term plus refrigeration) electric powers required to operate the PF magnetic coil system

P_{repro} = power required to reprocess fuel on site

P_{BOP} = balance-of-plant power

$P_{p\text{-}reac}$ = total pumping power for the transmutation reactor

$P_{p\text{-}FW}$ = pumping power for the first wall

P_{other} = miscellaneous powers that are not accounted for explicitly.

Values for these powers and efficiency factors for the FTWR reference design are shown in Table XVII. Most of these values are calculated. However, some numbers (η_{th}, P_{tot}^{PF}, P_{repro}, P_{BOP}, P_{other}) have been estimated by direct scaling from comparable design studies. The values P_{repro} and P_{BOP} were estimated from a cost estimate of these same facilities for an ATW design.[48]

Using these values, the calculated electric power amplification factor Q_e for the reference design is ~1.0; i.e., the FTWR produces all the electricity that it needs to perform its mission, transmuting SNF.

In case one or more of the numbers in Table XVII turn out to be less favorable than anticipated, we can maintain electrical self-sufficiency by adding fuel assemblies to the fission reactor to increase the power output. This is demonstrated in Table XVIII, where the electric power amplification factor Q_e is calculated for the reference design with one-half and one additional rows of fuel assemblies. The power requirements increase slightly (only the P_{BOP}, P_{repro}, and $P_{p\text{-}reac}$ terms would increase), so the excess electricity raises the value of Q_e. It can be seen that there is enough margin to accommodate reasonable uncertainties in the powers and efficiencies listed in Table XVII.

TABLE XVII

Reference Design Powers and Efficiencies

P_{fus} (MW)	150
P_{reac} (MW)	3000
P_{tot}^{TF} (MW)	656
P_{tot}^{CS} (MW)	216
P_{tot}^{PF} (MW)	100
$P_{p\text{-FW}}$ (MW)	2.5
$P_{p\text{-}reac}$ (MW)	131
P_{repro} (MW)	23
P_{BOP} (MW)	6
P_{other} (MW)	5
η_{th} (%)	40
η_{CD}^{e} (%)	70

TABLE XVIII

Effects of Added Fuel Assemblies

Added Rows	0	$\frac{1}{2}$	1
P_{fus} (MW)	150	150	150
P_{reac} (MW)	3000	3600	4200
Q_e (MW)	1.0	1.17	1.33

This calculation also suggests that the FTWR can produce surplus electricity by increasing the number of fuel assemblies. For example, if the FTWR operated at 6 GW(thermal), the resulting Q_e would be equal to 1.77, resulting in ~1 GW(electric) of surplus electricity.

X. CONCLUSIONS AND DISCUSSION

The first major conclusion of this study is that an FTWR based on liquid metal–metal fuel fast reactor technology and a D-T tokamak fusion neutron source is a feasible option for substantially reducing the quantity and hazard potential of high-level radioactive waste from SNF that must be stored in geological repositories. An FTWR that produces 3000 MW(thermal) would transmute the transuranic content of ~100 metric tonnes of SNF per FPY and would be self-sufficient in producing all the tritium and electricity required for its operation. By repeated recycle of transuranics from SNF in a series of FTWRs, >99% of the transuranics would be destroyed by fission. One FTWR operating with 60% availability would support three commercial LWRs [1000 MW(electric) each], so that an equilibrium fleet of 34 FTWRs [3000 MW(thermal) each] would support the present U.S. commercial nuclear capacity of 100 GW(electric). This same support level applies also to a mix of FTW and ATW reactors.

The second major conclusion is that a fusion neutron source that met all the requirements, except high availability, for an FTWR could be designed and built today, based on the existing tokamak physics and fusion technology databases. The plasma confinement and stability parameters needed in an FTWR ($H \geq 1$, $\beta_N \approx 2.5$) are routinely achieved in operating tokamaks. The required plasma current, plasma energy amplification factor, and auxiliary heating power ($I_p = 7$ MA, $Q_p = 1.5$ to 2, $P_{aux} \approx 80$ MW) are only modest extrapolations from existing tokamaks. Empirical scaling laws predict that

steady-state current drive can be achieved with these parameters, based on experience in existing tokamaks. The resistive magnet and liquid nitrogen cooling technology to achieve 8- to 10.5-T fields is well established. The tritium processing system technology that has been developed for JET and TFTR and in the ITER R&D program should provide an adequate design base for the FTWR. The remote handling technology that has been developed in the ITER R&D program should provide an adequate design base for the fusion neutron source for the FTWR.

The third major conclusion is that availability is the major issue for the FTWR. The equilibrium transuranic inventory (hence the repository requirement) and the size of the FTWR fleet needed to achieve this equilibrium inventory are sensitive to the availability of the FTWR. Achieving an availability of >50% in the second generation of FTWRs is important. Since we have based the FTWR design on the nuclear and processing technology that is being developed in the U.S. fast reactor program for the ATW, we assume the same high availability for the transmutation reactor in the FTWR as is anticipated in the ATW design. Thus, the availability of the FTWR will be determined by the availability of the fusion neutron source.

There are two elements to the issue of availability of the fusion neutron source: (a) reliable, high availability, routine operation of the neutron source and (b) downtime for the replacement of failed components. Both of these issues suggest the need to build a prototype tokamak fusion neutron source as soon as possible to learn how to achieve a routine high availability operation and to learn about any short-term failure modes of the components.

This leaves the issue of long-term component failure due to radiation damage, which is common to all transmutation reactors and other devices with a high neutron fluence mission. The most inaccessible components in the FTWR, the toroidal and CS magnets, are shielded sufficiently to be lifetime components. However, some structural components (e.g., the first wall of the neutron source and the clad and structure in the reactor fuel assemblies) will accumulate high levels of radiation damage. The radiation damage limit for the HT-9-like steel components is not known, but estimated lifetimes in a fusion neutron spectrum are in the range of 100 to 200 dpa. These damage limits would require that first wall of the fusion neutron source be replaced 2 to 4 times during the 40-FPY lifetime of an FTWR. Since the wall replacement could be scheduled to coincide with a plan outage for refueling it should not have a substantial impact on average lifetime availability, even if first-wall lifetimes <100 are encountered.

We tried to make this initial assessment of an FTWR realistic by basing the design concept for the neutron source on the existing tokamak physics and fusion technology databases and by basing the design concept for the transmutation reactor on the nuclear and processing technology that is being developed for the ATW reactor. The major uncertainties in this existing database vis-à-vis the FTWR requirements are in the areas of high availability, steady-state tokamak operation, and structural materials lifetime, as discussed earlier, and only the former would substantially impact availability. However, there will inevitably be design-specific R&D requirements identified by a more detailed assessment of the FTWR at the conceptual design level that includes the mechanical and thermal designs of the magnet systems, the transmutation reactor, the fuel changeout and reprocessing systems, etc., and the safety and environmental analysis.

APPENDIX A

PLASMA PHYSICS ANALYSIS

A.I. CONFINEMENT[19]

The ITER Database IPB98(y,2) scaling is used:

$$\tau_E = H\tau_E^{\mathrm{IPB98}(y,2)} \ , \tag{A.1}$$

where

$$\tau_E^{\mathrm{IPB98}(y,2)} = 0.144 I_p^{0.93} B_0^{0.15} P^{-0.69} \bar{n}_{e20}^{0.41} \times M^{0.19} R_0^{1.97} A^{-0.58} \kappa^{0.78} \ , \tag{A.2}$$

and the units are in s, MA, T, MW, 10^{20} m^{-3}, amu, and m.

A.II. GREENWALD DENSITY LIMIT

$$\bar{n}_{e20} \le \frac{I_p\,(\mathrm{MA})}{\pi a^2} \ . \tag{A.3}$$

A.III. L-H MODE TRANSITION THRESHOLD[19]

$$P_{LH}\,(\mathrm{MW}) = (2.84/M) B_0^{0.82} \bar{n}_{e20}^{0.58} R_0 a^{0.81} \ . \tag{A.4}$$

A.IV. MHD STABILITY

$$\beta_t \equiv \frac{\langle n_e T_e + n_i T_i + p_\alpha \rangle}{\dfrac{B_0^2}{2\mu_0}} \le \beta_N \frac{I_p\,(\mathrm{MA})}{aB_0} \tag{A.5}$$

and

$$q_{95} = \frac{5a^2 B_0}{R_0 I_p} \frac{1 + \kappa^2(1 + 2\delta^2 - 1.2\delta^3)}{2} \times \frac{\left(1.17 - \dfrac{0.65}{A}\right)}{\left(1 - \dfrac{1}{A^2}\right)^2} \ge 3 \ . \tag{A.6}$$

A.V. BOOTSTRAP CURRENT FRACTION[49]

$$f_{bs} = C_{BS}(\sqrt{\epsilon}\beta_p)^{1.3} \ , \qquad \text{(A.7)}$$

where

$$C_{BS} = 1.32 - 0.235q_{95} + 0.0185q_{95}^2 \qquad \text{(A.8)}$$

and

$$\beta_p = \beta_t(B_0/B_p)^2 \ , \quad B_p = \frac{I_p\,(\text{MA})}{5a\sqrt{\dfrac{1+\kappa^2}{2}}} \ . \qquad \text{(A.9)}$$

A.VI. FAST WAVE ICRF CURRENT DRIVE EFFICIENCY[22]

$$\gamma_{FW} \equiv R_0\, n_{e20}\, \eta_{\text{CD}} = 0.062T_e\,(\text{keV})^{0.56} \ , \qquad \text{(A.10)}$$

where $\eta_{\text{CD}} = I_{\text{CD}}\,(\text{MA})/P_{aux}\,(\text{MW})$ is the current drive efficiency.

A.VII. VOLT-SECOND ANALYSIS

Volt-seconds required for startup, $\Delta\Phi_{start} = (\Delta\Phi)_{ind} + (\Delta\Phi)_{res}$, where

$$(\Delta\Phi)_{ind} = I_p L_p \qquad \text{(A.11)}$$

and

$$(\Delta\Phi)_{res} = C_{Ejima}\,\mu_0 R_0 I_p \ , \qquad \text{(A.12)}$$

where the Ejima coefficient is assumed to be equal to 0.4 (Ref. 49).

$$L_p = \mu_0 R_0\left[\ln\left(\frac{8R_0}{a\sqrt{\kappa}}\right) + \frac{l_i}{2} - 2\right] \qquad \text{(A.13)}$$

and the internal inductance l_i is given by[50]

$$l_i = \ln(1.65 + 0.89(q_{95} - 1)) \ . \qquad \text{(A.14)}$$

APPENDIX B

MATERIALS PROPERTIES

Coolants		
Properties	Li17PB83 (Ref. 51)	LBE (Ref. 52)
Density (kg/m^3)	9270	10 190
Resistivity (Ω·m)	9.71×10^{-8}	4.29×10^{-7}
Specific heat, C_p (J/kg·K)	187	129
Viscosity (mPa·s) at 698 K	1.39×10^6	1.46×10^6

HT-9 (Ref. 53)	
Property	Value
Yield strength (MPa)	307
Ultimate strength (MPa)	396
Thermal conductivity (W/m·K)	30
Poisson's ratio	3
Density (kg/m^3)	9270
Resistivity (Ω·m)	1.32×10^{-6}

OFHC	
Property	Value
Resistivity (Ω·m) at 100 K[a]	0.36×10^{-8}
Yield strength at 100 K (MPa)	370
Ultimate strength at 100 K (MPa)	470

LN_2 (Ref. 26)	
Property at 70 K	Value
Density (kg/m^3)	840.0
Specific heat, C_p (J/kg·K)	2024
Viscosity, μ (μPa·s)	220
Thermal conductivity, k (W/m·K)	0.150

[a]A temperature-dependent model for the OFHC resistivity was used.[54]

APPENDIX C

MAGNET ANALYSIS

C.I. CS COIL

C.I.A. Volt-seconds

$$(\Delta\Phi)_{\text{CS}} = \pi B_{OH} R_{fc}^2\left[1 + \frac{\Delta_{OH}}{R_{fc}} + \frac{1}{3}\left(\frac{\Delta_{OH}}{R_{fc}}\right)^2\right] \ , \qquad \text{(C.1)}$$

where

B_{OH} = magnetic field at the CS

R_{fc} = flux core radius

Δ_{OH} = radial thickness of CS.

Equation (C.1) assumes linear decay of the magnetic field within the CS cross section.

C.I.B. Tensile Stress[55]

$$\sigma_{\text{CS}} = \frac{B_{OH}^2}{2\mu_0}\left(\frac{R_{fc}}{\Delta_{OH}} + \frac{1}{3}\right) \le S_m \ , \qquad \text{(C.2)}$$

where, according to the ASME code, $S_m = \min\left[\frac{1}{3}\text{ ultimate stress}, \frac{2}{3}\text{ yield stress}\right]$. For composite materials, the maximum stress S_m is estimated from

$$S_m = \sum_i f_i \times S_{mi} \ , \tag{C.3}$$

where S_{mi} is the maximum allowable stress of material i and f_i is the volume fraction of material i.

C.II. TF COILS

C.II.A. Centering Force[55,56]

$$F_R = \frac{\mu_0 N I_{TF}^2}{2}\left[1 - \frac{1}{\sqrt{(1-\epsilon_p^2)}}\right] \ , \tag{C.4}$$

where

N = number of TF coils

I_{TF} = current per TF coil

$\epsilon_p = R_{bore}/R_0$, where R_{bore} is the radius of the magnet bore.

C.II.B. Bending Stress

$\sigma_{bend} = F_R/A_{in}$, where A_{in} is the area of the inner leg of the magnet over which the inward force acts.

C.II.C. Tensile Force[55,56]

$$F_T = \frac{1}{2}\frac{\mu_0 N I_{TF}^2}{4\pi}\ln\left(\frac{1+\epsilon_p}{1-\epsilon_p}\right) \ , \tag{C.5}$$

and the corresponding tensile (hoop) stress is equal to

$$\sigma_t = F_T/A_{tor} \ , \tag{C.6}$$

where A_{tor} is the cross-sectional area of conductor plus structure but not including the coolant channels. According to the ASME code, $\sigma_t + \sigma_{bend} \le 1.5 S_m$, where S_m is defined as in the preceding.

APPENDIX D

PUMPING POWER CALCULATIONS

The flow rate through each region is determined from the heat removal requirement

$$P_{th} = \dot{m} C_p \Delta T = \rho v A C_p \Delta T \ , \tag{D.1}$$

where

P_{th} = thermal power (W)

$\dot{m}$ = mass flow rate (kg/s)

C_p = 1000 (33.77–0.00158 T (K))/173.156 = heat capacity of the coolant (J/kg·K)

v = flow velocity (m/s)

A = cross-sectional flow area (m^2).

The pumping power is determined for each component of the pressure drop using

$$P_{p,x} = \frac{\Delta p_x A v}{\eta} \ , \tag{D.2}$$

where η is the pumping efficiency and Δp_x is the result pressure drop from losses from the x component.

The friction pressure drop is determined[56] from

$$\Delta p_{fric} = f L_c \rho v^2/2D \ , \tag{D.3}$$

where

$f = 0.0014 + 0.125(Dv\rho/\mu)^{-0.32}$

D = 4 A/wetted perimeter = hydraulic diameter

$\mu = 0.187 e^{11\,640/8.314T(\mathrm{K})}$ = viscosity (mPa·s).

The pressure drop from potential energy gains or gravity was determined using

$$\Delta p_g = \rho g h \ , \tag{D.4}$$

where h is the elevation change of the vertical flow through the region.

The MHD pressure drop is calculated using[56]

$$\Delta p_{\mathrm{MHD}} = L_c V B_r^2 \sigma_f \frac{C}{1+C} \ , \tag{D.5}$$

where

L_c = flow length for the path

B_r = magnetic field in region r perpendicular to the flow

σ_f = conductance of the cladding (1/Ω·m)

$C = \dfrac{2\sigma_s t}{\sigma_f D}$

σ_s = conductance of the liquid metal coolant (1/Ω·m)

t = thickness of the cladding (m).

APPENDIX E

TRITIUM ANALYSIS

The time dependent tritium inventory is given by

$$\frac{dT(t)}{dt} = (1-\alpha)\dot{T}(t) - \dot{F}(t) - \lambda_T(t)$$

$T(t)$ = tritium inventory

α = tritium reduction factor

$\dot{T}(t)$ = tritium production rate

$\dot{F}(t)$ = fusion rate

λ_T = tritium decay constant

Limit

$$T_{\text{EOC}} \geq T_{\text{BOC}}\, e^{\lambda_T t_{down}}$$

T_{BOC} = startup tritium inventory

T_{EOC} = tritium inventory at EOC

t_{down} = down time between cycles.

The tritium production rate is reduced by the α term that takes into account all losses other than decay as well as uncertainties in the reactions rates and geometrical modeling errors. The methodology, model, and values used to estimate α were based on the model developed in Ref. 57. The preceding equation expresses the cumulative nonradioactive losses for and infinite number of passes through the plasma. Table E.I shows the values of the parameters defined in Ref. 57 used to estimate the nonradioactive loss of tritium. The total nonradioactive losses are estimated at 2.3%. There are significant uncertainties in the parameters used to estimate the losses.

The tritium production rate also needs to be reduced by an amount to account for uncertainty in the calculated tritium production rate. This is very difficult to estimate because these errors result from errors in the neutron spectrum resulting from cross-section errors. The geometry model is also a very simplified model of the actual geometry, which produced additional errors in the tritium production rate. A total reduction in the tritium production rate of 7% was used to estimate the tritium inventory. Since tritium self-sufficiency is a requirement, the uncertainty in tritium production rate translates into an uncertainty in the lithium enrichment required to achieve tritium self-sufficiency.

TABLE E.I

Tritium Loss Model Parameters

Parameter	Value	Definition
ϵ_1	0	Loss in blanket
ϵ_2	0.001	Loss in breeder processing
ϵ_4	0	Loss in fuel cleanup and isotope separation
β	0.05	Fractional burnup in plasma
f_l	0.0001	Leakage from plasma to limiter
f_{fw}	0.0001	Leakage from plasma to first wall
ϵ_6	0.001	Loss in plasma exhaust processing
α''	0.02346	Fraction of tritium atoms produced that will be lost

APPENDIX F

TRANSMUTATION ANALYSIS

The transmutation analysis is performed by two different code packages. The REBUS fuel cycle code[37] performs the FTWR transmutation calculations. The fission products are treated as several lumps in the REBUS calculations. The SCALE 4.4 code[44] was used to determine the composition of the fission product lumps and to calculate the LWR SNF composition.

The REBUS fuel cycle is run in two different modes. The first mode is the enrichment search for the equilibrium fuel cycle. The second mode is the nonequilibrium or depletion mode to determine the behavior of the FTWR over the equilibrium cycle.

For the equilibrium calculations, the BOC target k_{eff} (0.95) and all fuel cycle parameters (e.g., cycle length, power level, recovery fraction, and SNF feed composition) are specified along with the initial guess at the equilibrium enrichment. The REBUS code calculates the flux distribution and reaction rates at BOC, and depletes the fuel to the next time step. The flux distribution and reaction rates are then calculated at the end of the time step, and the code then adjusts the transmutation matrix and new compositions are calculated for the end of the time step. This process continues until EOC is reached. The EOC composition is then processed according to the external cycle parameters, the recovered material is combined with makeup from the LWR SNF feed and a new estimate of BOC concentration and enrichment is made. The cycle transmutation calculations are then repeated. The code then iterates until the enrichment is determined for the equilibrium cycle and the concentrations of materials in the equilibrium fuel cycle have converged.

A smaller number of time steps are required in the equilibrium cycle iterations than is necessary to accurately integrate some of the time dependent parameters such as the tritium inventory. To reduce the calculation time, the equilibrium cycle enrichment search is run using a smaller number of time nodes and then a single depletion calculation is performed with a larger number of time nodes. The BOC fuel concentration is depleted under the same conditions as the equilibrium calculations, except more neutron transport calculations are performed over a cycle, which provides the fission rate, tritium production rate and other data at more points throughout the cycle.

To greatly reduce the calculation time, the number of isotopes in the transmutation matrix can be reduced by lumping the fission products. In a fast spectrum, there are not any fission products with huge cross sections like xenon and samarium in an LWR. There are ten fission product lumps used in this analysis. Each fission produces two fission product lumps, one for rare earth fission products, a fraction of which are recycled with transuranics, and one for the nonrare earth fission products. These

fission product lumps are based on the equilibrium fission product concentration for ^{235}U, ^{238}U, ^{239}Pu, ^{240}Pu, and ^{241}Pu in a fast spectrum. The fission of other isotopes is assumed to produce the fission products for the isotope with the closest mass. The equilibrium composition of the hundreds of isotopes in the lumps is estimated using the SCALE 4.4 code package[44] with its standard fast reactor cross sections. These compositions are then used to produce multigroup cross sections for the ten fission product lumps. For the toxicity calculations, the toxicity is assumed to be that of the isotopic mixture used to produce the fission product lumps.

NOMENCLATURE

ANL = Argonne National Laboratory

ATW = accelerator transmutation of waste

BOC = beginning of cycle

B_4C = boron carbide

CS = central solenoid

EOC = end of cycle

FPD = full power day

FPY = full power year

FTWR = fusion transmutation of waste reactor

FW = fast wave

HT-9 = a ferritic steel alloy

ICRF = ion cyclotron range of frequency

JET = Joint European Torus

k_{eff} = effective neutron multiplication constant of a fissioning assembly

LBE = lead-bismuth eutectic

Li17Pb83 = lithium-lead eutectic 17 parts Li and 83 parts Pb

LN_2 = liquid nitrogen LN_2

LWR = light water reactor

MHD = magnetohydrodynamics

MT = metric tonne

MTU = metric tonne of initial uranium

OFHC = oxygen-free high conductivity copper

OTC = once-through fuel cycle

POPCON = Plasma Operating CONtour

Pyro = pyrometallurgical

Q_e = electric power amplification factor (electric power produced/electric power consumed)

Q_p = plasma energy amplification factor (fusion power/external heating power)

SNF = spent nuclear fuel

TF = toroidal field

TRU = transuranics

UREX = URanium EXtraction system

REFERENCES

1. "First Phase P&T Systems Study: Status and Assessment Report on Actinide and Fission Product Partitioning and Transmutation," OECD/NEA, Paris (1999).

2. *Proc. 1st through 5th NEA International Exchange Meetings*, OECD/NEA, Paris (1990, 1992, 1994, 1996, 1998).

3. "Nuclear Wastes—Technologies for Separations and Transmutations," National Research Council, National Academy Press, Washington (1996).

4. C. D. BOWMAN et al., "Nuclear Energy Generation and Waste Transmutation Using Accelerator-Driven Intense Thermal Neutron Source," *Nucl. Instrum. Methods A*, **320**, 336 (1992).

5. W. C. SAILOR et al., "Comparison of Accelerator-Based with Reactor-Based Nuclear Waste Transmutation Schemes," *Prog. Nucl. Energy*, **28**, 359 (1994).

6. "A Roadmap for Developing Accelerator Transmutation of Waste (ATW) Technology," DOE/RW-0519, U.S. Department of Energy (1999).

7. T. A. PARISH and J. W. DAVIDSON, "Reduction in the Toxicity of Fission Product Wastes Through Transmutation with Deuterium-Tritium Fusion Neutrons," *Nucl. Technol.*, **47**, 324 (1980).

8. E. T. CHENG et al., "Actinide Transmutation with Small Tokamak Fusion Reactors," *Proc. Int. Conf. Evaluation of Emerging Nuclear Fuel Cycle Systems*, Versailles, France (1995).

9. Y.-K. M. PENG and E. T. CHENG, "Magnetic Fusion Driven Transmutation of Nuclear Waste (FTW)," *J. Fusion Energy*, **12**, 381 (1993).

10. E. T. CHENG and R. J. CERBONE, "Prospect of Nuclear Waste Transmutation and Power Production in Fusion Reactors," *Fusion Technol.*, **30**, 1654 (1996).

11. Y. GOHAR, "Fusion Option to Dispose of Spent Nuclear Fuel and Transuranic Elements," ANL/TD/TM00-09, Argonne National Laboratory (2000).

12. L. J. QIU et al., "A Low Aspect Ratio Tokamak Transmutation System," *Nucl. Fusion*, **40**, 629 (2000).

13. W. M. STACEY, "Capabilities of a DT Tokamak Fusion Neutron Source for Driving a Spent Nuclear Fuel Transmutation Reactor," *Nucl. Fusion*, **41**, 135 (2001).

14. ITER TEAM, "ITER Physics Basis," *Nucl. Fusion*, **39**, 2137 (1999).

15. F. ENGELMANN, "Steady-State Operation of Magnetic Fusion Devices," *Nucl. Fusion*, **40**, 1025 (2000).

16. R. R. PARKER, "ITER In-Vessel System Design and Performance," *Nucl. Fusion*, **40**, 473 (2000).

17. W. S. YANG and H. KHALIL, "ATW System Point Design Employing LBE Cooled Blanket Design," Argonne National Laboratory (2000).

18. D. E. POST, N. A. UCKAN, and the U.S. ITER HOME TEAM, "Criteria and Design Trade-Off Issues for ITER," *Fusion Technol.*, **21**, 1427 (1992).

19. Y. SHIMOMURA et al., *Nucl. Fusion*, **41**, 309 (2001).

20. L. GIANCARLI, "Water-Cooled Pb-17Li Demo Blanket Line EU Reference Conceptual Design and Performance Presentation," DMT 94/538 (SERMA/LCA/1678), Commissariat à l'Energie Atomique (1994).

21. T. S. TAYLOR, *Plasma Phys. Control. Fusion*, **39**, B47 (1997).

22. T. K. MAU, University of California, San Diego, Personal Communication (Apr. 2001).

23. S. C. JARDIN et al., *Fusion Eng. Design*, **38**, 27 (1997).

24. A. TANGA et al., "A High Performance and Long Pulse Tokamak," EURATOM-ENEA (1991).

25. T. BROWN et al., "Fusion Ignition Research Experiment (FIRE) Engineering Status Report" (Oct. 2000).

26. R. D. WOOLLEY, "Long Pulse Fusion Physics Experiments Without Superconducting Electromagnets," *Fusion Technol.*, **34**, 543 (1998).

27. M. SAWAN, Personal Communication (Mar. 2001).

28. L. A. EL-GUEBALY, H. Y. KHATER, and the ARIES TEAM, "Need for Inboard Shield to Protect the Center Post of ST Power Plants," *Fusion Technol.*, **34**, 1089 (1998).

29. M. E. SAWAN and H. Y. KHATER, "Nuclear Analysis of the FIRE Ignition Device," UWFDM-1134, Madison, Wisconsin (Oct. 2000).

30. W. REIERSEN et al., *Proc. Symp. Fusion Engineering*, Institute of Electrical and Electronics Engineers, p. 1035 (1998).

31. R. D. LEGETT and L. C. WALTERS, "Status of LMR Fuel Development in the US," *J. Nucl. Mater.*, **204**, 23 (1993).

32. D. C. NORRIS, W. M. STACEY, M. YAKSH, S. M. GHIASIAAN, "First-Wall Material/Coolant Heat Flux Limit Comparison," *Fusion Technol.*, **34**, 924 (1998).

33. S. MORI et al., "Blanket and Divertor Design for the Steady State Tokamak Reactor (SSTR)," *Fusion Eng. Des.*, **18**, 219 (1991).

34. F. NAJMABADI et al., "Titan Reversed-Field-Pinch Fusion Reactor Study," UCLA-PPG-1200, University of California, Los Angeles (1990).

35. M. E. SAWAN and I. N. SVIATOSLAVSKY, "Assessment of First Wall Lifetime in D-^{3}He and D-T Reactors with Impact on Reactor Availability," *Fusion Technol.*, **26**, 1141 (1994).

36. R. N. HILL and H. KHALIL, "ATW System Point Design Employing Sodium Cooled Blanket Design," Draft ATW Report, Argonne National Laboratory (July 21, 2000).

37. B. J. TOPPEL, "A User's Guide to the REBUS-3 Fuel Cycle Analysis Capability," ANL-83-2, Argonne National Laboratory (1983).

38. "DANTSYS: A Diffusion Accelerated Neutral Particle Transport Code System," LA-12969-M MANUAL UC-705, Los Alamos National Laboratory (Mar. 1997).

39. H. HENRYSON II et al., "MC^2-2: A Code to Calculate Fast Neutron Spectra and Multigroup Cross Sections," ANL-8144, Argonne National Laboratory (1976).

40. W. M. STACEY, Jr., B. J. TOPPEL, H. HENRYSON II, B. A. ZOLOTAR, R. N. HWANG, and C. G. STENBERG, "A New Space-Dependent Fast-Neutron Multigroup Cross Section Processing Capability," *Trans. Am. Nucl. Soc.*, **15**, 292 (1972).

41. D. S. GELLES, "Microstructural Examination of Commercial Ferritic Alloys at 200 DPA," Semiannual Progress Report, DOE/ER-0313/16, U.S. Department of Energy (1994).

42. F. NAJMABADI et al., "ARIES-I Tokamak Reactor Study Final Report," UCLA-PPG-1323, University of California, Los Angeles (1991)

43. R. N. HILL, "LWR Feed Inventory Specifications for ATW System Studies," internal memo, Argonne National Laboratory (June 12, 2000).

44. "SCALE: A Modular Code System for Performing Standardized Computer Analyses for Licensing Evaluation," NUREG/CR-0200, Rev. 5 (ORNL/NUREG/CSD-2/R5), Vols. I, II, and III, Oak Ridge National Laboratory/U.S. Nuclear Regulatory Commission (Mar. 1997).

45. "Draft Environmental Impact Statement for a Geologic Repository—Appendix A: Inventory and Characteristics of Spent Nuclear Fuel, High-Level Radioactive Waste, and Other Materials," DOE/EIS-0250D, U.S. Department of Energy Office of Civilian Radioactive Waste Management (July 1999).

46. ATW SEPARATIONS TECHNOLOGIES AND WASTE FORMS TECHNICAL WORKING GROUP, "A Roadmap for Developing ATW Technology: Separations and Waste Forms Technology," ANL-99/15, Argonne National Laboratory (Aug. 1999).

47. "Integrated Data Base Report—1996: US Spent Nuclear Fuel and Radioactive Waste Inventories, Projections, and Characteristics, 1–7," DOE/RW-0006, U.S. Department of Energy (1997).

48. M. R. SHAY et al., "Life-Cycle Cost Analysis for Developing and Deploying a Representative Accelerator Transmutation of Waste System," PNNL-SA-32548, Pacific Northwest National Laboratory (Jan. 2000).

49. "ITER Physics," ITER Documentation Series, No. 21, International Atomic Energy Agency (1991).

50. J. WESSON, *Tokamaks*, 2nd ed., Oxford, United Kingdom (1997).

51. STI/PUB-795, INTOR Phase 2A, Part III, Vol. 1, p. 444, International Atomic Energy Agency (1988).

52. INTERNATIONAL NUCLEAR SAFETY CENTER, available on the Internet (http://www.insc.anl.gov/matprop/pbbi/pbbi.html) (http://www.insc.anl.gov/matprop/pbbi/pbbiviscosity.pdf).

53. R. L. KLUEH, Oak Ridge National Laboratory, Personal Communications (data from *Nuclear Systems Materials Handbook*, Rev. 2).

54. P. TITUS, Massachusetts Institute of Technology, Personal Communication.

55. R. J. THOME and J. M. TARRH, *MHD and Fusion Magnets*, Wiley-Interscience, New York (1982).

56. W. M. STACEY, Jr., *Fusion*, Wiley Interscience, New York (1984).

57. M. A. ABDOU, E. L. VOLD, C. Y. GUNG, M. Z. YOUSSEF, and K. SHIN, "Deuterium-Tritium Fuel Self-Sufficiency in Fusion Reactors," *Fusion Technol.*, **9**, 250 (1986).

Weston M. Stacey (PhD, nuclear engineering, Massachusetts Institute of Technology, 1966) is a Callaway Regents' Professor of Nuclear Engineering at Georgia Institute of Technology (Georgia Tech). His current research interests are plasma theory and experimental analysis and fusion neutron source applications.

John Mandrekas (PhD, nuclear engineering, University of Illinois at Urbana-Champaign, 1987) is a senior research scientist of the Fusion Research Center at Georgia Tech. His research interests are nuclear fusion, applied plasma physics, computational physics, and numerical methods.

Edward A. Hoffman (PhD student, nuclear and radiological engineering, Georgia Tech) is a research assistant in the Fusion Research Center at Georgia Tech. His research interest is transmutation of nuclear waste.

G. P. Kessler (BSNRE, Georgia Tech, 2001).
C. M. Kirby (BSNRE, Georgia Tech, 2001).
A. N. Mauer (BSNRE, Georgia Tech, 2001).
J. J. Noble (BSNRE, Georgia Tech, 2001).
D. M. Stopp (BSNRE, Georgia Tech, 2001).
D. S. Ulevich (BSNRE, Georgia Tech, 2001).